Impervious Surface Cover Change in the Lower Mekong Region from Daytime and Nighttime Satellite Data (2001-2012)

January 2018

Pok Sophak

Impervious Surface Cover Change in the Lower Mekong Region from Daytime and Nighttime Satellite Data (2001-2012)

A Dissertation Submitted to
the Graduate School of Life and Environmental Sciences,
the University of Tsukuba
in Partial Fulfillment of the Requirements
for the Degree of Doctor of Philosophy
(Doctoral Program in Integrative Environment and Biomass Sciences)

Pok Sophak

Table of Contents

Abstract

Impervious Surface Cover Change in the Lower Mekong Region from Daytime and Nighttime Satellite Data (2001-2012)

Pok Sophak

Impervious surface area (ISA), which is defined as the human-made surfaces that water cannot infiltrate into the soil, is an important indicator of urbanization as well as environmental quality in a drainage basin. Frequent updates of the amount and spatial distribution of ISA can help us understand the human-nature interaction and adverse impacts of ISA on the environment. This information has become increasingly useful for policy-makers, environmental managers and scientists. Although over the past three decades satellite data have been widely used to estimate ISA, it is still a challenge to estimate ISA at a large/regional spatial scale. There remain limitations in the previous methods considering image processing time, cost and ability to quickly map and update ISA. Thus, the objectives of this research are: 1) to develop an easily implemented method for estimating ISA on a large scale using Moderate Resolution Imaging Spectroradiometer (MODIS) and improved Defense Meteorological Satellite Program's Operational Line-scan (DMSP-OLS) nighttime light data (NTL); and 2) to evaluate the applicability of the developed method for estimating ISA in the lower Mekong region from 2001 to 2012 and analyze ISA changes and its impacts on drainage basin health.

A method for estimating ISA for the lower Mekong region was developed by using MODIS and improved DMSP-OLS NTL data. The method involved four major steps. First, a non-vegetation fraction map was generated from time-series MODIS Normalized Difference Vegetation Index (NDVI) data using temporal mixture analysis (TMA). The non-vegetation contains ISA and bare land because both land cover types have similar NDVI temporal profiles. Second, the enhanced-vegetation-index-adjusted nighttime light index (EANTLI) was used to overcome the saturation and blooming effects in the DMSP-OLS nighttime light data. Third, the

relationship between ISA% and EANTLI was derived based on a statistical analysis of the non-vegetation fraction image and the EANTLI image to obtain a preliminary ISA% map. There were two relationships found between ISA% and EANTLI in the study area: the natural logarithmic function is suitable for ISA% values between 0% and 50%; and the quadratic polynomial function should be used for ISA% values greater than 50%. Fourth, the final ISA% map was obtained by selecting smaller values from the preliminary ISA% map and non-vegetation fraction map for each pixel. This is because the non-vegetation land cover contains both ISA and bare land, and thus the ISA% should not exceed the fraction of non-vegetation. The validation results for 2001 showed that the proposed method has promising accuracy, with a root mean square error (RMSE) value of 0.111, a systematic error (SE) value of 0.061, and a determination coefficient of 0.87. The key element of the method lies in building relationships between ISA% and EANTLI. To build the relationship, previous studies generally selected calibration area and used Landsat or high spatial resolution images to generate reference ISA. It can be considered choosing the calibration area to represent the whole region is problematic and that generating reference ISA data for a large scale study is labor-intensive and time-consuming, making it difficult to update the ISA maps. The proposed method just used MODIS and DMSP-OLS nighttime light data, so it is relatively simple and easy to implement.

The proposed method was then applied to MODIS and DMSP-OLS NTL data to produce the annual ISA% maps from 2001 to 2012 and to detect ISA change in the lower Mekong region. In this application, the comparability and consistency of the time-series DMSP-OLS NTL data, which are the inputs in the fourth step of the developed method, need to be taken into account. The raw DMSP-OLS NTL images were captured from different satellites at different years. These data are incomparable and cannot be directly used for change analysis due to lack of on-board calibration in the OLS sensors, sensor degradation, satellite shift and atmospheric effects. To address this issue, inter-calibration of the time-series DMSP-OLS NTL images was carried out using a stepwise calibration method. In addition, further temporal correction was implemented to

the inter-calibrated NTL images by using an assumption that NTL detected in the previous year would not disappear in the later years. In estimating annual ISA, the two relationships (natural logarithmic and second order polynomial functions) between ISA% and EANTLI were found in all the years. The resulted ISA% maps from 2001 to 2012 were used to assess ISA change in the lower Mekong region as a whole and for each country. The regional ISA increased significantly from 29,398 km^2 (1.7% of the total land area) in 2001 to 47,635 km^2 (2.8%) in 2012, indicating large urban expansion over the period. An increasing trend was observed in the whole study area and each country (R^2>0.67). The average annual growths of ISA were estimated at 56 km^2/year, 89 km^2/year, 442 km^2/year and 829 km^2/year for Laos, Cambodia, Vietnam and Thailand respectively. Overall, the ISA increase was at an alarming rate that would cause concern about its effects on the environment.

The impacts of ISA on the drainage basins' health in the region were identified based on the percentage of ISA in each basin. Of a total of 847 drainage basins, there were 524 (61.9%) in no_impact category, 280 (33.1%) in stressed category, 40 (4.7%) in impacted category and 3 (0.4%) in degraded category in 2001. The number of basins within stressed, impacted and degraded increased category to 372 (43.9%), 57 (6.7%) and 7 (0.8%) respectively in 2012. In contrast, the number of drainage basins in no_impact category decreased from 524 (61.9%) in 2001 to 411 (48.5%) in 2012. ISA at both the region and the country levels is on an increasing trend due to development pressure, suggesting that there is an urgent need to take appropriate measures to control ISA growth to protect the basins' quality in the region.

Keywords: Impervious surface area, temporal mixture analysis, MODIS, DMSP-OLS nighttime light, EANTLI, drainage basin quality.

List of Tables

List of Figures

List of Abbreviations

Abbreviation	Explanation
ANN	Artificial Neural Network
ASTER	Advanced Spaceborne Thermal Emission and Reflection Radiometer
AVHRR	Advanced Very High Resolution Radiometer
DMSP	Defense Meteorological Satellite Program
DN	Digital Number
EANTLI	Enhanced-Vegetation-Index-Adjusted Nighttime Light Index
EVI	Enhanced Vegetation Index
GDP	Gross Domestic Product
GPS	Global Positioning System
HSI	Human Settlement Index
ISA	Impervious Surface Area
MESMA	Multi-Endmember Spectral Mixture Analysis
MNF	Minimum Noise Fraction
MODIS	Moderate Resolution Imaging Spectroradiometer
MRC	Mekong River Commission
NASA	National Aeronautics and Space Administration
NDVI	Normalized Difference Vegetation Index
NDWI	Normalized Difference Water Index
NOAA	National Oceanic and Atmospheric Administration
NPP	National Polar-Orbiting Partnership
NSMA	Normalized Spectral Mixture Analysis
NTL	Nighttime Light
NUACI	Normalized Urban Areas Composite Index

N-V	Non-vegetation
OLS	Operational Line-scan
PNMESMA	Pre-screened and Normalized Multiple Endmember Spectral Mixture Analysis
RMSE	Root Mean Square Error
SE	Systematic Error
SMA	Spectral Mixture Analysis
SPOT	Satellite Pour l’Observation de la Terre
TMA	Temporal Mixture Analysis
VANUI	Vegetation-Adjusted Nighttime Light Urban Index
VIIRS	Visible Infrared Imaging Radiometer Suite
V-I-S	Vegetation-Impervious Surface-Soil
WGS84	World Geodetic System 1984

Chapter 1

Introduction

1.1 Background

With population growth and socioeconomic development, the world has been rapidly urbanizing over the past century. Urban population increased from 30% (746 million) of the total world population in 1950 to 54% (3.9 billion) in 2014 and is projected to grow up to 66% by 2050 (UN, 2014). Although the global urban area is small, urbanization is among the most important human impacts that affects land use and land cover change, which triggers environmental changes locally and globally (Grimm et al., 2008; Murayama et al., 2016). Obviously, due to rapid urbanization considerable amounts of forest and agricultural lands have been replaced by housings, shopping malls, factories, commercial and administrative buildings, roads, parking lots and other human-man features to support the increasing socioeconomic demands. These human-made surfaces, which prevent water from infiltrating into the soil, are defined as impervious surface area (ISA) (Arnold and Gibbons 1996; Xian et al., 2007).

Impervious surface area serves as an index of urban development. The amount of impervious surfaces can quantitatively describe the level of urbanization or how dense an urban area is. Past studies have shown the positive correlation between impervious surface percentage and population density in urban areas and used impervious surfaces to estimate population distribution (Novak and Greenfield, 2012; Zhu et al., 2015). In addition, impervious surface area is regarded as an important indicator of environmental quality (Anold and Gibbon, 1996). In general, as the impervious surface cover increases, the speed and volume of stormwater runoff increase and the runoff brings nonpoint source pollutants from various land uses into water bodies, such as rivers, streams and lakes. Consequently, the water quality becomes degraded. The impacts of impervious

surfaces on hydrological processes in watersheds have been confirmed by many studies (Schueler, 1994; Jacobson, 2011). It was also found that the increase in impervious surfaces in the watersheds can increase the risk of flood disaster as it has greatly increased peak discharge and flood volume (Du et al., 2015). Furthermore, impervious surfaces can alter local temperature and cause heat islands effects in urban areas (Grimm et al., 2008; Buyantuyev and Wu, 2010; Li et al., 2011). The two factors can influence building energy use and human health (Novak and Greenfields, 2012). As increased impervious surfaces cause a reduction in natural land cover as well as alterations of hydrological and thermal characteristics in watersheds, biodiversity and ecosystem functions are also affected (Matsushita et al., 2014). Given the important role the impervious surfaces play, estimating ISA and understanding the spatial distribution and change of impervious surface cover have become increasingly important for urban planners, watershed managers, policy makers, scientists and other stakeholders.

Since 1970s, various remote sensing satellites have been launched to the space to collect information on the Earth. Those satellites include Landsat, SPOT, ASTER, AVHRR, DMSP, MODIS, IKONOS, Quickbird, etc. The specifications of the satellite platform and the sensors onboard determine the spatial, spectral, temporal and radiometric resolutions of the captured images (Le Moigne et al., 2011). With these characteristics, remote sensing satellite data can be used to extract different useful information related to land use and land cover change, weather, climate, ecosystem and other fields to support decision making and benefit our society. Remarkably, ISA, the most important human footprint on the Earth, can be extracted from satellite images. Between early 1970s and 1990s, efforts to extract and estimate ISA from remote sensing data (particularly Landsat) were reported; yet there were only a small number of studies due to lack of satellite data with suitable characteristics for estimating ISA, lack of advanced image processing techniques and limited computing power (Slonecker et al., 2001; Weng, 2012). Since 2000s, estimating ISA from remote sensing has gained widespread interests from scientific community, and the number of studies on ISA including methods and applications has

considerably increased. As reviewed by Weng (2012) there has been clearly significant development in methods to estimate ISA from different satellite data with spatial resolution ranging from high (e.g. IKONOS, QuickBird), medium (Landsat MMS, TM, ETM+) to low (e.g. MODIS, AVHRR, DMSP-OLS). The methods have also shifted from using conventional supervised and unsupervised classification to sub-pixel mapping approach.

The discovery of vegetation-impervious surface-soil (V-I-S) model for characterizing urban/near-urban environment (Ridd, 1995) has opened the door for the application of spectral mixture analysis (SMA) approach to estimate ISA. Based on the proposed V-I-S model, Wu and Murray (2003) employed Landsat ETM+ and SMA method to estimate ISA in a study area of 81 square kilometers within the metropolitan area of Columbus, Ohio United States. In their study, ISA endmember was represented by a sum of high albedo and low albedo. Later, Wu (2004) extended the method to a normalized spectral mixture analysis (NSMA) applied to Landsat ETM+ to reduce brightness variation with each V-I-S component. The normalized spectra allowed a single endmember to represent each component. Lu and Weng (2006) were successful in extracting impervious surface information from Landsat ETM+ data based on the integration of fraction images from linear spectral mixture analysis and land surface temperature. Powell et al. (2007) developed a method called multiple endmember spectral mixture analysis (MESMA). MESMA models spectra as the linear sum of spectrally pure endmembers that vary on a per pixel basis. Spectral variability was reduced by allowing the number and type of endmembers to vary from pixel to pixel. In their work, MESMA and Landsat ETM+ were used to produce a set of maps representing per-pixel fraction of each component (V-I-S) in the city of Manaus, Amazonas, Brazil. This method involved constructing endmember library, applying simple SMA model to each pixel, selecting best model for each pixel. The models were generalized into the land cover components of interest (i.e. V-I-S) and an image of fractional coverage per pixel was generated for each component. Later, Yang et al. (2010) estimated the ISA at the drainage basin level (Lake Kasumigaura) in Japan using Landsat 5 TM images. They developed a pre-screened and

normalized multiple endmember spectral mixture analysis (PNMESMA) method, which improved endmember selection technique and combined NSMA with MESMA. In selecting vegetation endmember, two additional datasets of NDVI (>0.5) and reflectance at red band (<0.07), were used to extract pure pixel. For low albedo, high albedo and soil, only the endmember pixels selected from the feature space representations of the reflectance image were used.

The advantage of this SMA method is that it can solve mixed-pixel problem in the image. However, SMA suffers from spectral similarity among non-vegetation land cover classes and spectral variability with endmembers (Somers et al., 2011; Yang et al., 2012). Later, with the advent of MODIS, which provides high temporal resolution images, a number of studies have focused on using this rich temporal information to estimate ISA (Knight and Voth, 2011; Shao and Lunetta, 2011; Yang et al., 2012; Li and Wu, 2015). Shao and Lunetta applied multi-layer perceptron neural network to time-series MODIS NDVI to map ISA at sub-pixel level. Knight and Voth (2011) investigated the use of time-series MODIS NDVI data to estimate ISA in a major metropolitan area of Minnesota, USA. They experimented two years and four years of 16-day composited MODIS NDVI in the pixel unmixing method to estimate ISA and found almost no difference in mapping accuracies between the two experiments. Although the successes of these methods to map ISA have been presented, the accuracies remained a big challenge. The selection of time series data as input into the method were suggested as critically important for improving the accuracy of ISA estimates. Yang et al. (2012) proposed a temporal mixture analysis (TMA) method to estimate ISA in Japan using a sorted temporal profiles of time-series MODIS NDVI data. The sorting procedure reduced endmember variability within each land cover class and yielded a more accurate estimation of ISA. Due to the coarse spatial resolution of MODIS data, it is possible to produce ISA maps over a larger area (e.g. regional and global). However, when estimating ISA for a large area, TMA is often sensible to the confusion between ISA and bare land because both of the non-vegetation land cover types have similar temporal profiles. In addition, regression analysis method is another mean to map ISA at sub-pixel level. This method was used

for estimating ISA percent based on vegetation fraction, reflectance spectra or nighttime light (Bauer et al., 2008; Weng and Hu, 2008; Elvidge et al., 2007; Lu et al., 2008).

A majority of the previous studies, particularly those that used SMA method have focused on small areas such as a city or a watershed. For estimating ISA on a large scale (i.e., regional or global), the use of high or medium spatial resolution data can be considered ineffective and impracticable due to the excessive amount of processing time, computer capacity, labor and cost involved. The coarse spatial resolution satellite data from MODIS and DMSP-OLS NTL data have been used for estimating large-scale ISA with success (Yang et al., 2012; Yang et al., 2014; Elvidge et al., 2007; Lu et al., 2008). However, on one hand, TMA method applied to MODIS data suffers from the similarities between the temporal signature of bare land and ISA, which can reduce accuracy of estimated ISA. On the other hand, the regression analysis approach applied to DMSP-OLS NTL data suffers from the issue that only part of the study area or a number of selected samples are used to generate the regression model and cannot well represent the whole study area. Moreover, reference ISA data for the calibration area or samples usually are estimated from Landsat images or high spatial resolution images, which is laborious and difficult to frequently update ISA in other years. With regard to the DMSP-OLS NTL data, the effects of blooming and saturation can limit the usefulness of the data or can affect accuracy of ISA estimation.

As ISA serves as a significant indicator to explain watershed health, frequent updates of ISA information can be used to identify the status of watersheds and track the shift in severity of the affected watersheds. However, there is a lack of ISA data produced with frequent updates and sufficient geographic coverage to analyze the change of status of watersheds containing in a large region or the world. For example, Elvidge et al. (2007) produced a global ISA map of 2000-2001 from DMSP-OLS nighttime light and population data. Since the regression analysis method was used in this study, the reference ISA data different years are required to update ISA map. Deriving the reference ISA data is a difficult task which restricts the ability to frequently updating ISA map. Yang et al. (2010) established a database of ISA for Lake Kasumigaura basin for 1987, 2000 and

2007 from Landsat images and analyzed the impacts on the basin. The analysis revealed that the basin were in the impacted category and will be in the degraded category in 2017 if the ISA continues to increase. The study was at a basin scale and ISA at only three single time periods were maps. Kuang et al. (2013) produced ISA maps for 2000 and 2008 to assess the impact on watersheds in China. However, there is a lack of such research on the ISA effects on watersheds in Southeast Asia although the region has been experiencing rapid urbanization, economic development and population growth over the past several decades. In particular, in four countries of the region (Laos, Thailand, Cambodia and Vietnam) which share the Mekong River as a vital water resource and share economic growth, it is necessary to look into the recent changes of ISA at different spatial scales (regional, country and drainage basin). Although past studies have mapped ISA at a large spatial scale with success, the mapping process is often complicated and difficult to update ISA maps.

1.2 Literature review: remote sensing of impervious surface area

During the past three decades, numerous methods and techniques have been developed for estimating impervious surface area (ISA). Measuring on the ground using GPS is one technique that can directly obtain the amount of ISA in an area. Manually interpreting aerial photographs or very high resolution imagery is another technique to estimate ISA. Both techniques are straightforward and give the most accurate results, but they involve much labor, time and budget, and are difficult to apply for large areas. With the availability of medium and coarse spatial resolution satellite data, it has become possible to estimate ISA for a larger area or the globe. However, one of the main challenges is the accuracy as the mixed pixels generally are contained in those satellite images. The advancement in computing field has provided a variety of means and techniques to estimate ISA at sub-pixel level with acceptable accuracy, such as spectral mixture analysis and artificial neural network.

Table 1 describes the major methods used for estimating ISA from medium and coarse spatial resolution images. The methods can be divided into two major categories: empirical method and mixture analysis method.

1.2.1 Empirical methods

Bauer et al. (2008) estimated ISA by building a regression model between ISA percent and vegetation index or greenness by considering the inverse relationship between impervious surface and vegetation cover in urban areas. They used Landsat TM and ETM+ to estimate ISA for the state of Minnesota, USA, and model calibration sites were selected for each Landsat image with about 50 sites. The calibration sites were 40 to 100 Landsat pixels, or approximately 2.5 to 10 ha in size. The reference ISA of each site was digitized from 1-meter panchromatic digital orthophoto to determine the ISA percent in each site. Lu et al. (2008) developed a regression model for estimating ISA using an index called human settlement index. The index was calculated from a combination of DMSP-OLS NTL and MODIS NDVI images. The reference ISA data were derived from Landsat ETM+ and used as a dependent variable. The human settlement index was used as a single independent variable in the linear regression analysis. In addition, in order to generate the regression model, approximately 560 samples with a unit size of 1 km^2 were randomly selected from Landsat ETM+ images. Lee and Lathrop (2006) and Weng and Hu (2008) built a relationship between ISA percent and reflectance spectra using artificial neural network. Elvidge et al. (2007) built the global ISA estimation model from DMSP-OLS NTL data and population count data by using the USA as the calibration area. The reference ISA data for the entire USA were derived from Landsat images. The model for estimating the ISA was defined by linear regression and only grid cells with population count values of three or more were included in the regression. These empirical methods have the limitation that the model performance strongly depends on calibration data or area. If only one part of the study area or a selected number of samples is used to represent the whole region to generate the models, it is very difficult to judge how well the part or the

samples can represent the whole study area. Furthermore, high resolution images are required to obtain the reference ISA to be used as an input for generating the regression models. This process to derive ISA reference is usually time-consuming and labor-intensive.

1.2.2 Mixture analysis

Mixture analysis is a pixel unmixing approach to decompose mixed pixels in an image into different component fractions. There are two types of mixture analysis methods: spectral mixture analysis (SMA) and temporal mixture analysis (TMA). As the terms describe, SMA uses spectral information, while TMA uses temporal information and is the extended application of SMA. The SMA has been used widely used to estimate ISA (e.g. Wu and Murray, 2003; Wu, 2004, Lu and Weng, 2006, Powell et al, 2007; Yang et al., 2010). The method involves identifying reflectance spectra of pure land cover class called endmembers as inputs in SMA models. Landsat data has been popular in the SMA method because most studies focused on estimating or monitoring ISA in cities or watersheds. However, this method suffers from the confusion between non-vegetation land cover types (i.e. ISA and bare land) due to their spectral similarities. Furthermore, the spectral variability with endmembers is another issue in the SMA. With the availability of satellite data at high temporal frequency, TMA method has been applied to estimate ISA (Knight and Voth, 2011, Yang et al., 2012, Yang et al., 2014; Li and Wu, 2015). Although TMA method can reduce endmember variability with a land cover class by using a sorted temporal profile at higher section (Yang et al., 2012; Yang et al., 2014), it still suffers from temporal similarities between non-vegetation land cover types. Due to its high temporal resolution, MODIS has been widely used in the TMA to estimate ISA fraction.

Table 1 Major methods for estimating ISA percent at sub-pixel level from satellite sensors with medium to coarse spatial resolution

Category	Sub-category	Approach descriptions	Major limitations	References for example
Empirical method	Vegetation distribution-based	Building a relationship between ISA percent and vegetation indices (or greenness) by considering the inverse correlation between impervious surface and vegetation cover in urban areas.	Model performance strongly depend on calibration data.	Bauer et al. (2008) and Lu et al. (2008)
	ANN	Build a relationship between ISA percent and reflectance spectra using neural network techniques.	Model performance strongly depends on training data.	Lee and Lathrop (2006) and Weng and Hu (2008)
	Nighttime light-based	Build a relationship between ISA percent and DMSP-OLS data.	Model performance strongly depend on calibration data.	Elvidge et al. (2007) and Lu et al (2008)
Mixture analysis method	SMA	Estimate ISA percent using mixture analysis techniques based on spectral information obtained from satellite data.	Suffer from spectral similarity among non-vegetation land cover types and spectral variability within endmembers.	Wu and Murray (2003), Wu (2004), Lu and Weng (2006), Pwell et al. (2007), Yang et al., 2010
	TMA	Estimate ISA percent using mixture analysis techniques based on temporal information obtained from satellite data.	Suffer from temporal similarity among non-vegetation land cover types, and only suitable for coarse resolution satellite imagery.	Knight and Voth (2011), Yang et al. (2012), Yang et al. (2014), Li and Wu (2015)

ANN: artificial neural network; SMA: spectral mixture analysis; TMA: temporal mixture analysis

1.3 Originality and objectives of this research

The potential of satellite data with coarse spatial resolution, such as moderate resolution imaging spectroradiometer (MODIS) and Defense Meteorological Satellite Program's Operaltional Line-scan (DMSP-OLS) nighttime light (NTL) have been recognized for estimating ISA over a large area. The previous methods for estimating ISA on a large scale, such as SMA, TMA and regression analysis have been successful, yet there remain limitations (see Table 1). TMA outperforms SMA owing to its ability to reduce endmember variability within a land cover class. Nonetheless, TMA method, usually applied to MODIS data, suffers from the similarities between the temporal signatures of non-vegetation land cover types (mainly bare land and ISA), which can reduce accuracy of ISA estimates. Moreover, the regression analysis approach applied to DMSP-OLS NTL data suffers from the issue that only part of the study area or a number of selected samples are used to generate the regression model and cannot well represent the whole study area. The reference ISA data for the calibration area or samples are typically estimated from Landsat images or high spatial resolution images, which is laborious and difficult to frequently update ISA in other years. In addition, the effects of blooming and saturation in DMSP-OLS NTL data can limit the usefulness of the data and can affect ISA estimation. This present research utilized a combination of MODIS and DMSP-OLS NTL data to develop an easy-to-implement method for large-scale ISA estimation with particular focuses on addressing the issues of bare land and ISA confusion in TMA, representability of the calibration data/area, incorporating improved DMSP-OLS NTL data, and simplicity of the method to quickly and frequently update ISA maps.

MODIS and DMSP-OLS NTL data, which are readily available, can enable ISA mapping on an annual basis and temporal change analysis. The ISA information is critical for decision makers, urban planners, and scientists in related fields. However, the consistency/comparability of DMSP-OLS nighttime light time-series is an important consideration for dynamic study. Recently, a number of studies have shown significant development in improving the consistency of the global DMSP-OLS NTL time-series. Still, there may be region-specific aspects to further improve

the consistency of the NTL data for more accurately estimating ISA and analyzing its dynamics on a reginal scale. Until now, remote sensing community have generated a large amount of ISA data, but mostly for city or basin scale. In addition, global ISA maps were also produced but only a single year or two single years. The demand for frequent updates of ISA maps for monitoring ISA in a rapidly urbanizing region such as the lower Mekong region is increasing. In addition, the change in ISA will affect the drainage basins in the region, and it is very important to know the level of impacts in order to develop policies or take appropriate measures to reduce or prevent the degradation of the basins and water quality. Therefore, this research focused on evaluating the applicability of the developed method for annual mapping of ISA and using the annual ISA data to assess the change from 2001 to 2012 in the lower Mekong region and watershed health.

Consequently, the objectives of this research are: 1) to develop an easily implemented method for estimating ISA on a large scale using MODIS and improved DMSP-OLS NTL data; and 2) to evaluate the applicability of the developed method for estimating ISA in the lower Mekong region from 2001 to 2012 and analyze its changes and impacts on watershed health.

Chapter 2

Study area and datasets

2.1 Study area

The study area was a subset of a region in mainland Southeast Asia lying between latitudes 5º 25″ and 23º 33″ N, and longitudes 97º 3″ and 109º 47″E, with a total land area of approximately 1,716,000 square kilometers (Figure 2.1). The Mekong River, one of the world's major rivers, flows though this region. The study area not only covered the Lower Mekong Basin but also its surrounding area. This larger region was chosen in order to allow the boundary of four countries (Laos, Thailand, Cambodia and Vietnam) to completely contain in the region since one of the objective of this study was to make an analysis of ISA change at a country level. Because the study area was a region larger than the Lower Mekong Basin, it was named the "lower Mekong region" in for the purpose of easy description.

The lower Mekong region's climate is a tropical monsoon climate, which develops a bi-seasonal pattern of wet and dry periods during the year. The dry season, with no or little rainfall, is generally between mid-October and May, and the wet season, with high rainfall, starts in June and ends in October. The rainfalls in the region vary temporally and geographically. The highest monthly rainfall is usually observed in August or September. In terms of mean annual rainfall, Cambodia has the highest rainfall of more 1900 mm/year, while Thailand has the lowest of about 1600 mm/year. The annual average temperature of the region in general ranges from 22 ºC to 28 ºC, despite some variations with the latitude and altitude. The average monthly temperatures normally reach the maximum of 35 degrees Celsius at altitudes of less than 500 meters above mean sea level, and the minimum of 18 degrees Celsius during December and January (MRC, 2010). The land use in the region can be classified three broad types: paddy fields, mixed forests, and land cultivated for cash crops (MRC, 2011).

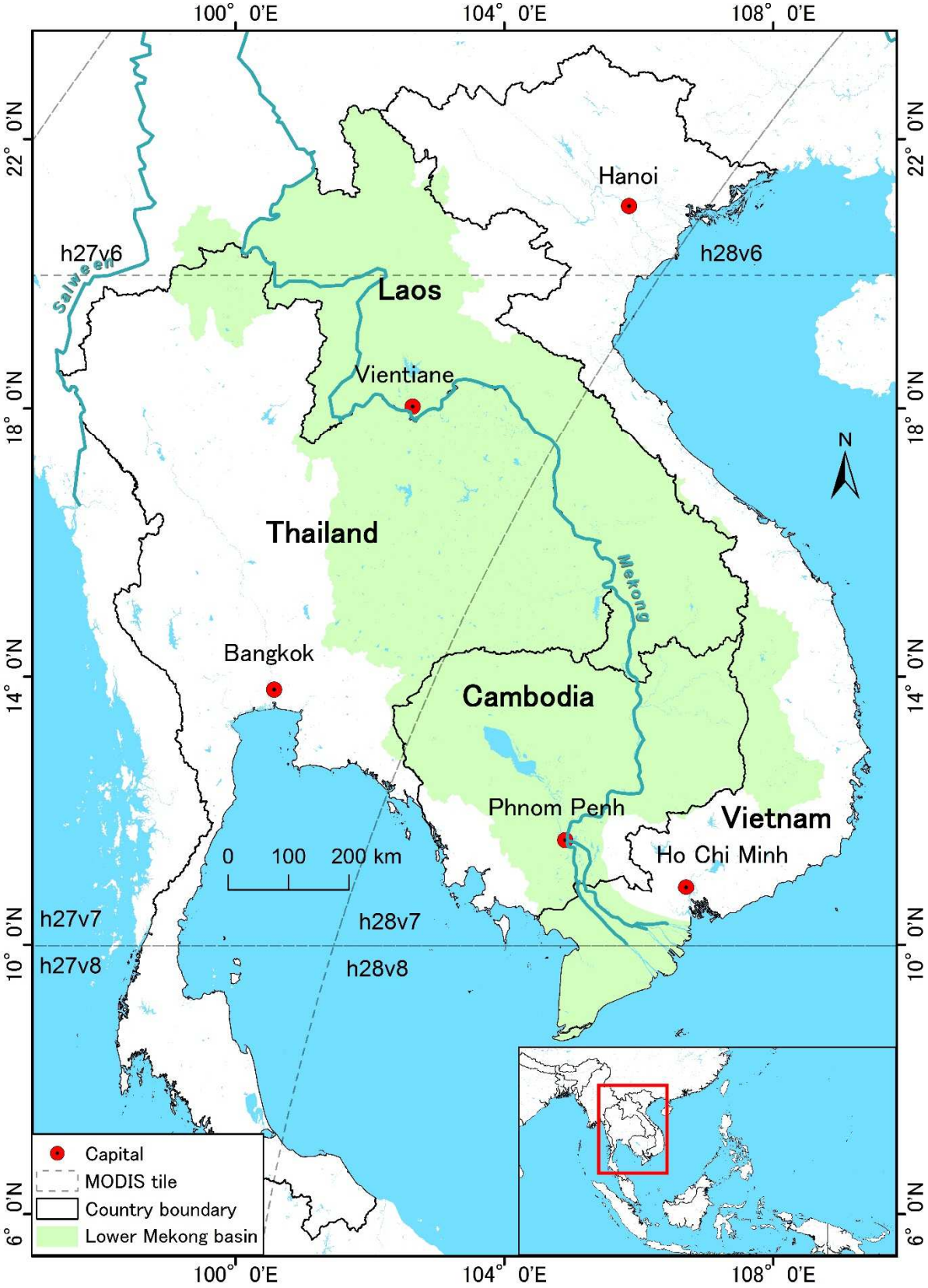

Figure 2. 1 Study area: the lower Mekong region

The lower Mekong region has experienced significant population and economic growth over the past quarter century. Figure 2.2 shows the population and growth domestic product (GDP) for Cambodia, Laos, Thailand and Vietnam. At the beginning of the 21st century the total population of the four countries reached 158 million, and the number increased to 184 million in 2016 (an increase of approximately 16%). Vietnam has the largest population, followed by Thailand, Cambodia and Laos. The GDP for each country has also increased remarkably. Thailand showed the highest GDP among the four countries and a dramatic growth, with the value increasing more than four times from 85.3 billion US dollars in 1990 to 406.8 US dollars in 2016. Notably, the total GDP of the four countries has risen very fast over the past 15 years. Overall, the trends of both population and GDP are predicted to continue to increase in the future. The fast growing number of people and economic activities undoubtedly brings with it rapid urbanization and associated issues such as land use/land cover change, degradation of environmental quality and loss of ecosystem function. Because of these changes, the amount of ISA will undoubtedly increase. Over the past 15 years, both the economy and population of the countries in the region have increased substantially. Therefore, knowing how much and where the ISA has increased over this period is extremely important for the regional management and planning. More frequently produced ISA maps (e.g. yearly or seasonally) would provide better analyses and enable better planning in the region.

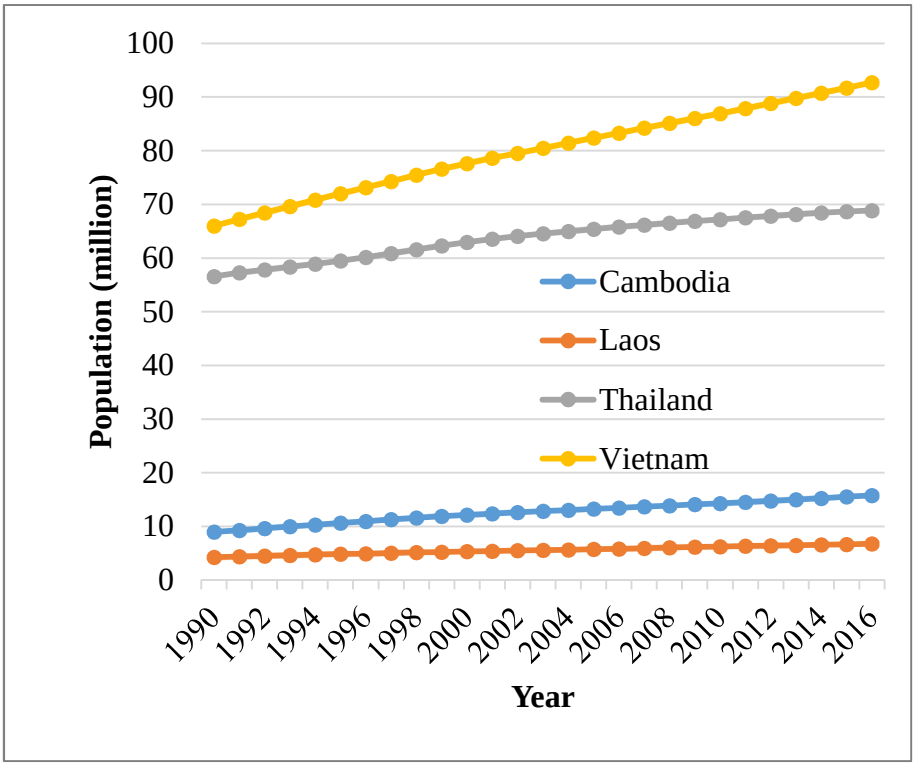

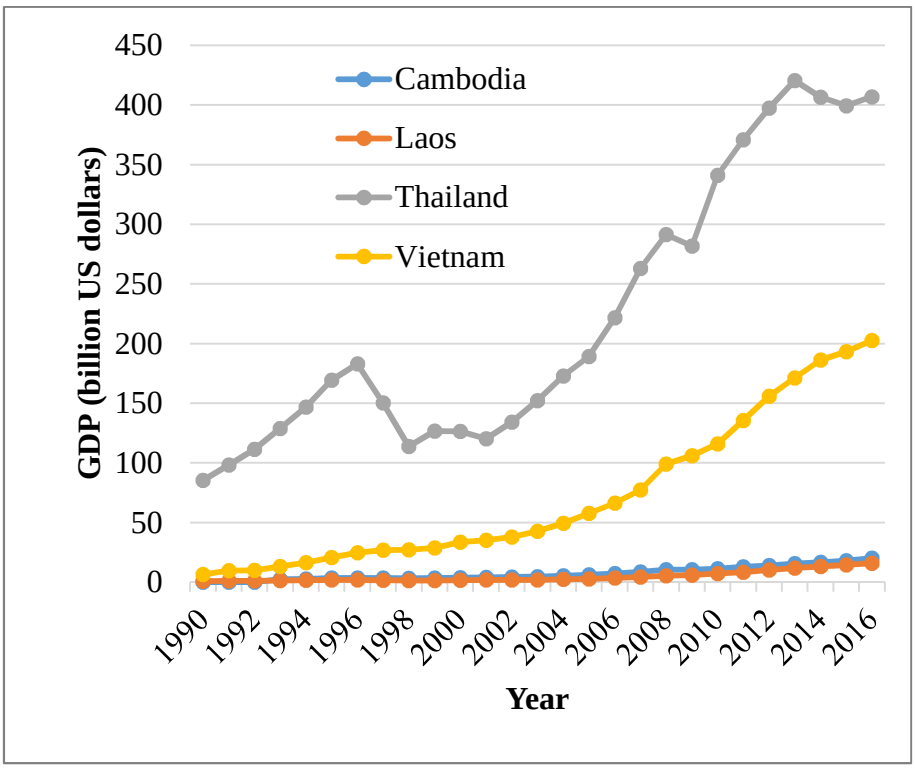

Figure 2. 2 World population and GDP for Cambodia, Laos, Thailand and Vietnam 1990-2016

(Source: World Bank, https://data.worldbank.org/)

2.2 Datasets

In this research, daytime satellite data, nighttime satellite data were primarily used for mapping ISA and monitoring its changes from 2001 to 2012. Remote sensing satellites are collecting information of the Earth 24 hours a day. Due to different specifications of sensors mounted on the satellites, they can provide various information of the Earth during both daytime and nighttime. The daytime data are in the form of spectral reflectance, which can be converted to indices such as NDVI. The daytime data are useful for distinguishing different land use and land cover types, while the nighttime data can provide information of night lights illuminated on Earth. The nighttime lights, largely from the human settlements, are very useful for identifying impervious surface area.

2.2.1 Daytime satellite data

The daytime satellite data used in this study were MODIS vegetation indices. MODIS is a sensor aboard the Terra and Aqua satellites. The satellites are viewing the entire Earth's surface every 1 to 2 days, acquiring data in 36 spectral bands (or groups of wavelengths). These MODIS data are playing a critical role in and will improve humans' understanding of global dynamics and processes occurring on the land, in the oceans, and in the lower atmosphere. All the MODIS datasets used in this study were downloaded from NASA website through the online Reverb tool (https://reverb.echo.nasa.gov/reverb/). MODIS NDVI data are from MOD13A2 product which is a 16-day composite, and MODIS EVI data are from MOD13A3 product which is a monthly composite of the highest quality pixels from daily images. These MODIS data have a spatial resolution of 1 km.

2.2.2 Nighttime satellite data

The nighttime satellite data used in this study are from Defense Meteorological Satellite Program's (DMSP) Operational Lines-can (OLS). Active for more than three decades, DMSP-

OLS was originally designed to observe global moonlit cloud information (Elvidge et al., 1997). The instrument has two spectral broad bands: visible and infrared, and collects images across a 3000 km swath width, providing coverage of the entire Earth twice per day. The low-light-sensing capacity of the DMSP-OLS sensor enables the detection of artificial lights at night (Elvidge, 2007; Zhang and Seto, 2011). The overpass time of the OLS sensor was during 20:30-21:30 local time every day (Bennett and Smith, 2017). The nighttime lights are from human settlements, gas flares, fires, and floating boats. The DMSP-OLS nighttime light data from 1992 to 2013 acquired by six different satellites namely F10, F12, F14, F15, F16 and F18, were processed and archived by National Geophysical Data Center of the National Oceanic and Atmospheric Administration (NOAA) (https://ngdc.noaa.gov/eog/dmsp/downloadV4composites.html). The archived data, known as stable lights, are annual cloud-free composites of global DMSP-OLS nighttime light images. The nighttime light data have digital number (DN) values ranging from 0 to 63 and a spatial resolution of 1 km.

Chapter 3

Development of a method to estimate impervious surface area on a large scale

3.1 Introduction

The term *impervious surface area* (ISA) describes the area of all the human-made surfaces on the Earth, including rooftops, roads, sidewalks, parking lots and so on. These human-made surfaces prevents water from infiltrating into the soil, and thus has different surface characteristics from natural land cover. Increases in the impervious surface area (ISA) in a watershed has great influence on the hydrological and thermal characteristics of the watershed. Therefore, ISA is considered to be an indicator with which urbanization, watershed function (e.g., Arnold and Gibbons, 1996) and impacts of environmental factors on climatology stations (Gallo and Xian, 2016) can be evaluated.

Remote sensing techniques have been widely used to estimate ISA since the 2000s (see the extensive review by Weng, 2012). One challenge in applying these techniques is that many mixed pixels exist in satellite imagery, especially imagery with medium to coarse resolution. To solve this problem, a large number of studies on estimating ISA at a sub-pixel level have been conducted. In which, the mixture analysis technique is one of main approaches for remotely estimating ISA with medium to coarse resolution imagery (Weng, 2012). Generally, the mixture analysis technique can be further separated into two sub-categories: spectral mixture analysis (SMA) and temporal mixture analysis (TMA). The main difference between SMA and TMA is that the former uses spectral information while the latter uses temporal information for each endmember (i.e., pure land cover type). Because of the use of temporal information, the TMA can only be applied to satellite imagery with coarse resolution because the revisit time is longer for satellite imagery with medium to high spatial resolution. For example, Wu and Murray (2003) obtained the reflectance

spectra of four endmembers (i.e., vegetation, soil, impervious surface with low albedo, and impervious surface with high albedo) from a Landsat/TM image to estimate the ISA in an American city (an example of the use of SMA); Yang et al. (2012) obtained the temporal profiles of three endmembers (i.e., forest, crop, and ISA) from the moderate resolution imaging spectroradiometer (MODIS) normalized difference vegetation index (NDVI) time-series datasets to estimate the ISA for all of Japan (an example of the use of TMA). Compared to SMA, TMA can efficiently reduce endmember variability, which is one of the largest sources of error in mixture analysis, and thus achieve improved ISA estimation (Somers et al., 2011; Yang et al., 2012). However, TMA has usually suffered from bare land effects when it has been used to estimate the ISA in a large area that contains more than one non-vegetation land cover type, leading to an overestimation of ISA (Yang et al., 2014).

Nighttime light (NTL) data, which can be obtained from the Defense Meteorological Satellite Program's Operational Line-scan System (DMSP-OLS), is another data source that is widely used for estimating ISA (e.g., Elvidge et al., 2007) or improving ISA estimation (e.g., Lu et al., 2008; Yang et al., 2014). However, pixel saturation in city cores and pixel blooming in suburbs are two obstacles to the successful application of DMSP-OLS data. Recently, several attempts have been made to address this issue (Lu et al., 2008; Zhang et al., 2013; Zhuo et al., 2015; Liu et al., 2015). The common concept underlying these efforts is the generation of a new index using a combination of the DMSP-OLS NTL and MODIS data-based indices. For example, Lu et al. (2008) proposed a human settlement index (HSI) determined through the combined use of a normalized DMSP-OLS NTL and the maximum MODIS NDVI between April and October in 2000; Zhang et al. (2013) modified the HSI to develop the vegetation-adjusted NTL urban index (VANUI) to overcome the drawbacks of the HSI; Zhuo et al. (2015) developed another index by combining the DMSP-OLS NTL with the MODIS enhanced vegetation index (EVI), which was named the EVI-adjusted NTL index (EANTLI), to further improve the performance of the HSI and VANUI; in the same year, Liu et al. (2015) also reported a new index by combining the DMSP-

OLS NTL with the MODIS EVI and normalized difference water index (NDWI) and named it the normalized urban areas composite index (NUACI), which also showed better performance than the HSI and VANUI.

Coarse spatial resolution images are suitable for estimating ISA on a large scale (regional or global) because it doesn't require too much time and labor for processing these images and thus allows frequently updating a product (Xian and Homer, 2010). Another important thing is that the use of coarse spatial resolution images makes users can benefit the merits of the TMA. In addition, it can be considered that the saturation problems and blooming effects in the original DMSP-OLS NTL data will limit its usefulness, and the improved DMSP-OLS NTL data (i.e., EANTLI) will help us to more efficiently mitigate the bare land effects in TMA-based ISA estimation. Consequently, the objective of this study is to propose an easily implemented method that can accurately and easily estimate ISA on a large scale from MODIS time-series and the improved DMSP-OLS NTL data.

3.2 Datasets

3.2.1 MODIS data

Three MODIS products were used in this study. These products were all acquired from NASA website through online Reverb tool (https://reverb.echo.nasa.gov/reverb/), and reprojected using the MODIS Reprojection Tool to meet the projection of the DMSP-OLS NTL data (i.e., geographic projection with datum of WGS84). The first product was the MODIS 16-day composited NDVI with a spatial resolution of 1 km (MOD13A2) for 2001. There are 23 elements in total for one year which can provide temporal information about the land surface. The downloaded MODIS NDVI temporal profiles were stacked as one multi-layer file and further smoothed using a Savitzky-Golay filter-based method to minimize the remaining cloud/noise effects and/or effects caused by atmospheric variability and imperfect sensor calibration (Chen et

al., 2004). The smoothed NDVI data were then sorted in ascending order, and the last 12 maximum NDVI elements were extracted. This is because previous studies have shown that the sorted NDVI temporal profiles (especially for high NDVI value zones) can reduce endmember variability and thus result in more accurate estimation of ISA (Yang et al., 2012; Yang et al., 2014).

The second product was the MODIS monthly composited EVI with a spatial resolution of 1 km (MOD13A3). This product was used together with the DMSP-OLS NTL data to calculate the EANTLI (Zhuo et al., 2015). The third product was the MODIS Land Water Mask with a 250-m spatial resolution (MOD44W). This product was used to mask water pixels before the ISA estimation was performed.

3.2.2 DMSP-OLS NTL data

The global DMSP-OLS NTL stable light product of 2001 (version 4; geographic projection with datum of WGS84; spatial resolution: 1 km) from DMSP satellite F15 was downloaded from the NOAA website (http://ngdc.noaa.gov/eog/index.html). The area corresponding to the study area was then cut out. The effects of moonlight, stray light, clouds, ephemeral fires, and gas flares have been removed from the product to ensure that the lights were almost all from human settlements (Elvidge et al., 2007). The light saturation problem in urban centers and the blooming effects in suburban areas were mitigated by combining the data with MODIS EVI data (Zhuo et al., 2015).

3.2.3 Historical images from Google Earth

The reference ISA data for accuracy assessment were collected from high-resolution Google Earth images of 2001-2004. In total, 97 stratified random samples were collected in order to evaluate the accuracy of the ISA estimation in a full dynamic range (i.e., ISA between 0 and 100%). For each reference sample, a 3 km x 3 km sampling unit (corresponding to 3 x 3 pixels of MODIS products or DMSP-OLS NTL data) was utilized to reduce the impact of geometric errors

associated with different datasets. The 97 extracted sample polygons (3 km x 3 km) were then classified as ISA and non-ISA using the unsupervised classification method with visual interpretation or the visually digitizing method in ENVI 5.2. The ISA fraction was finally calculated for each reference sample.

3.3 Development of an easily implemented method for estimating ISA from MODIS and DMSP-OLS NTL data

A flowchart of the proposed method is shown in Figure 3.1. The method consists of four major steps, which will be described in details below.

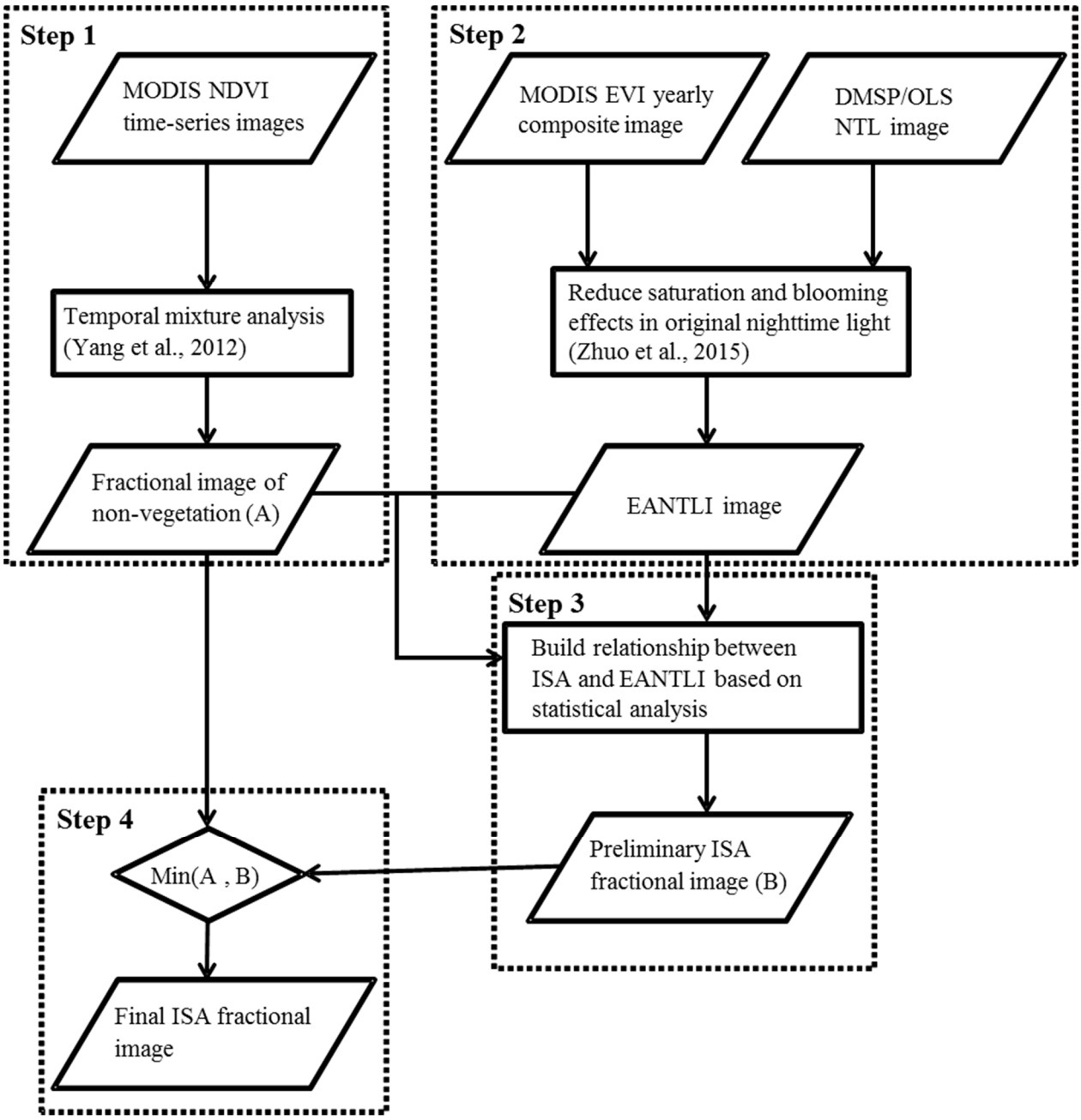

Figure 3. 1 Flowchart of the proposed method. Min (A, B) represents the selection of smaller value between images A and B.

3.3.1 Estimating the non-vegetation fraction from time-series MODIS NDVI data using the TMA method

In the TMA method, the NDVI value of a mixed pixel is considered to be the linear combination of the NDVI values of the endmembers and can be mathematically written as (Yang et al., 2012):

$$\mathrm{NDVI_{mix}} = \sum_{i=1}^{n} f_i \mathrm{NDVI_i} + \varepsilon \quad (1)$$

where $\mathrm{NDVI_{mix}}$ is the temporal profile of the NDVI of the target pixel, $\mathrm{NDVI_i}$ is the temporal NDVI signature of endmember i, f_i is the fraction of endmember i, and ε is the residual representing the model error. The fractions of the endmembers are commonly constrained by:

$$\sum_{i=1}^{n} f_i = 1 \text{ and } f_i \geq 0 \quad (2)$$

In this study, the fraction of each endmember was estimated using the constrained_min function in version 8.4 of the Interactive Data Language (IDL 8.4) software.

A minimum noise fraction (MNF) transform was carried out for the last 12 maximum NDVI values in sorted NDVI temporal profiles to facilitate the selection of endmembers. MNF transform is a linear transformation that consists of the two separate principal components analysis rotations. The first rotation uses the principal components of the noise covariance matrix to decorrelate and rescale the noise in the data, resulting in transformed data in which the noise has unit variance and no band-to-band correlations. The second rotation uses the principal components derived from the original image data after they have passed the first rotation and rescaled by the noise standard deviation. The inherent dimensionality of the data is determined by examining the final eigenvalues and the associated images. The lower MNF bands have spatial structure and contain most of the information. The scatter plots of the first three MNF bands were used to guide the selection of the endmembers (Figure 3.2).

From Figure 3.2, four endmembers were identified. They were forest, multi-crop, single-crop and non-vegetation (including ISA and/or bare land). The temporal profiles of the selected endmembers are shown in Figure 3.3. It can be seen that the NDVI temporal profile of forest showed almost no change at high NDVI values, whereas the NDVI temporal profile of non-vegetation showed almost no change, but showed low NDVI values. In contrast, the NDVI temporal profiles of crops (both single-crop and multi-crop) showed increasing trends in the NDVI values, which indicated the presence of phenological characteristics different from those of the other two endmembers (i.e., forest and non-vegetation).

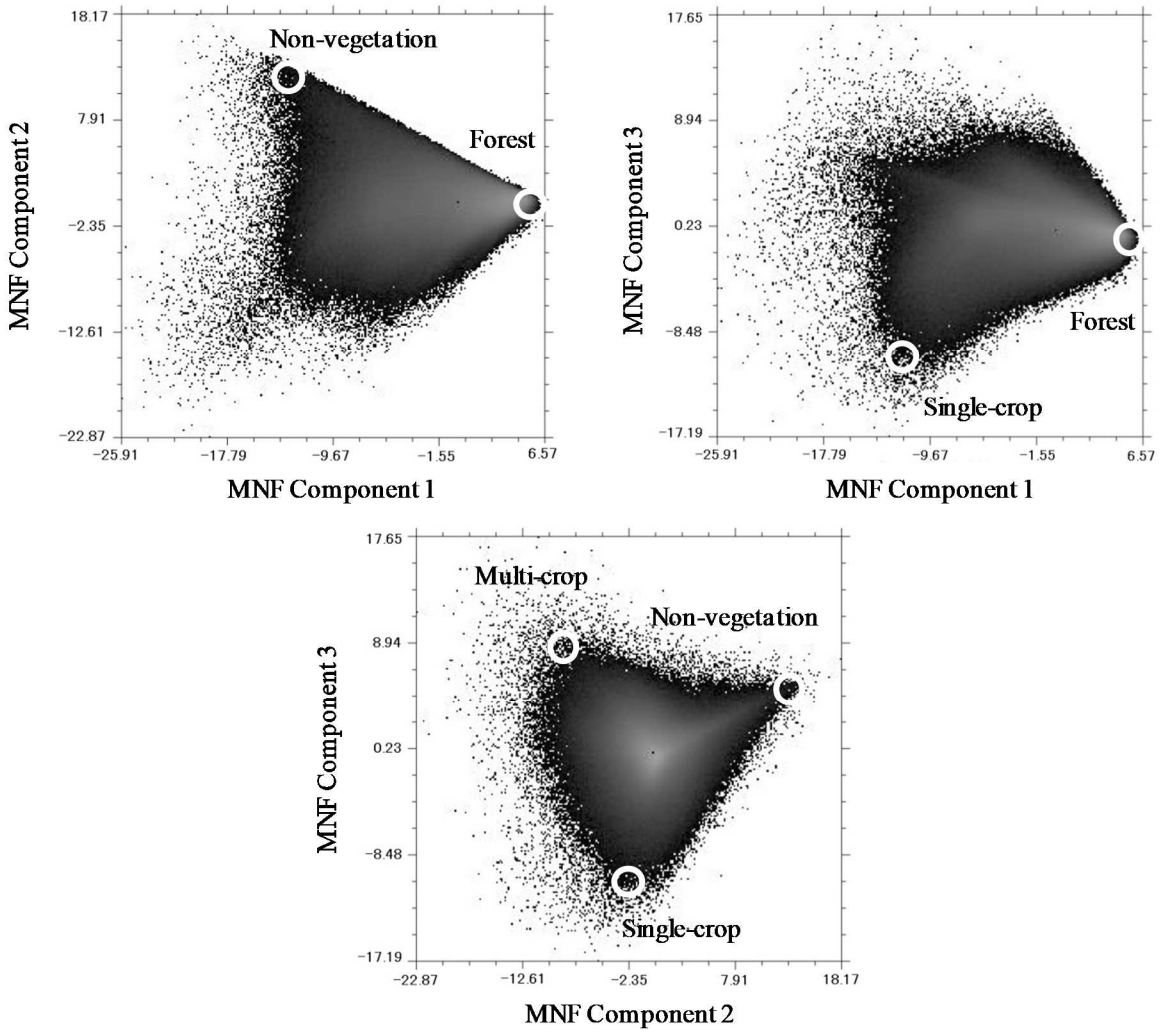

Figure 3. 2 Feature space representations of the first three minimum noise fraction (MNF) components.

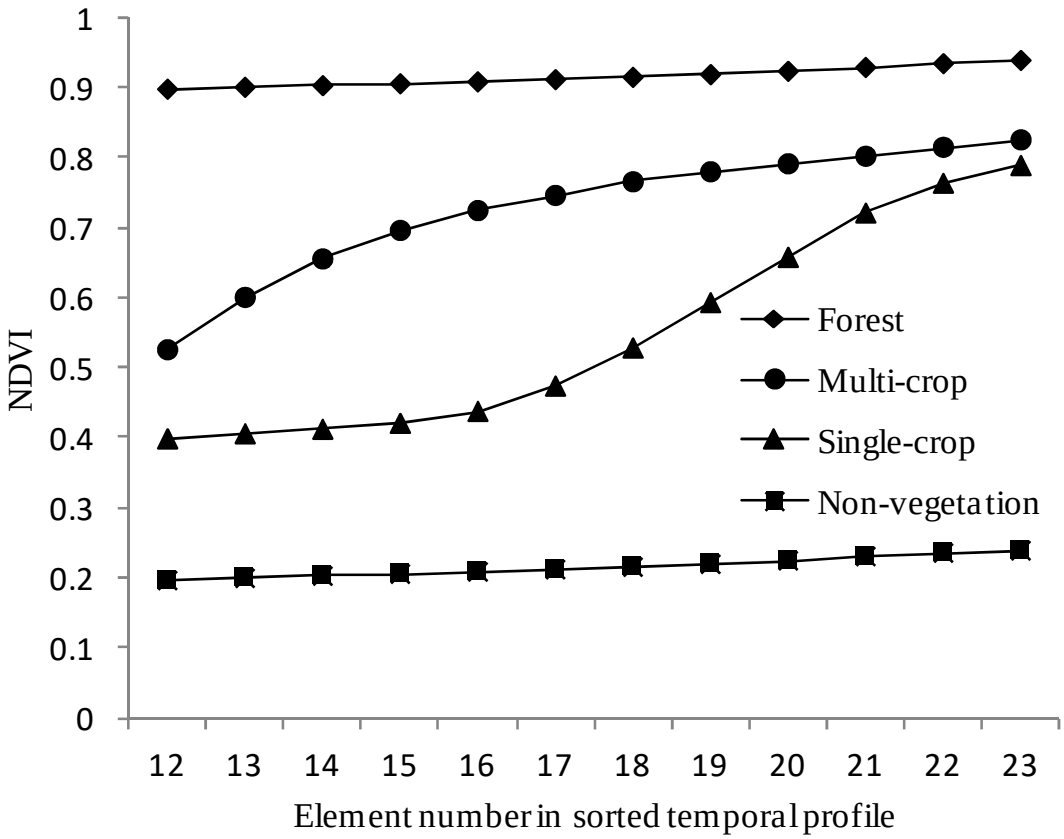

Figure 3. 3 NDVI temporal profiles of endmembers for temporal mixture analysis.

The fraction image of the non-vegetation endmember was calculated by Equation 1 using the constraints of Equation 2. In addition, since the purpose of this study was to estimate ISA, the pure vegetation pixels (i.e., pixels with NDVI values larger than 0.8 for all 12 elements) were identified and masked out before the fraction estimation to save computation time.

3.3.2 Calculating EANTLI from MODIS EVI and DMSP-OLS NTL data

The purpose of this step is to reduce the saturation and blooming effects in DMSP-OLS NTL images. These effects can restrict the ability of using the data for accurately estimating ISA. Blooming refers to the spurious indication of light in a location without a light source particularly in developed areas. The blooming is caused by three main phenomena: relatively coarse spatial resolution of OLS sensor and the detection of diffuse and scattered light over areas that have no

light source, a large overlap in the footprints of adjacent pixels, and the accumulation of geolocation errors in the compositing process. Saturation refers to the fact that data values in urban core areas is truncated due to 6-bit radiometric range of DMSP-OLS NTL (Small et al., 2005).

The EVI-adjusted NTL index (EANTLI) developed by Zhuo et al. (2015) is used to overcome the two main problems in the original DMSP-OLS NTL data (i.e., light saturation in urban centers and the blooming effect in suburban regions). It is known that the light saturation in urban centers conceals light intensity variations and spatial details, while the blooming effect leads to the overestimation of the lighted area in suburban regions (Lu et al., 2008; Zhang et al., 2013; Zhuo et al., 2015). Mathematically, the EANTLI can be written as (Zhuo et al., 2015):

$$\mathrm{EANTLI} = \frac{1 + \left((\mathrm{NTL})_{\mathrm{norm}} - (\mathrm{EVI})\right)}{1 - \left((\mathrm{NTL})_{\mathrm{norm}} - (\mathrm{EVI})\right)}(\mathrm{NTL}) \qquad (3)$$

where $(\mathrm{NTL})_{\mathrm{norm}}$ represents the normalized DMSP-OLS NTL value (divided by the maximum value of 63), (NTL) is the original DMSP-OLS NTL value, and (EVI) is derived from the monthly MODIS-EVI products. According to Equation 3, it is clear that the EANTLI can enlarge the original NTL digital number (DN) values when $(\mathrm{NTL})_{\mathrm{norm}}$ is larger than (EVI) (i.e., the potential saturated area) and reduce those NTL DN values when $(\mathrm{NTL})_{\mathrm{norm}}$ is smaller than (EVI) (i.e., the potential blooming area), and thus corrects the light saturation in urban centers and mitigates the blooming effects in suburban regions. The details of the rationality and performance of EANTLI can be found in Zhuo et al. (2015).

The EANTLI image was generated from the MODIS EVI product and DMSP-OLS NTL data using Equation 3.

3.3.3 Building a relationship between ISA and EANTLI

Figure 3.4 shows the results of a statistical analysis of the original and improved (i.e., EANTLI) DMSP-OLS NTL for 10 non-vegetation fraction groups ranging from 1% to 100% divided into deciles (i.e., 1-10%, 11-20%, 21-30%, 31-40%, 41-50%, 51-60%, 61-70%, 71-80%, 81-90% and 91-100%). The non-vegetation fractions were obtained from the results of Section

3.3.1. The NTL or EANTLI values from the lower to the upper limit at the 5th, 25th, 50th, 75th, and 95th percentiles are shown for each non-vegetation fraction group. Figure 3.4 shows that: (1) very low NTL or EANTLI values appeared even for some pixels with a higher non-vegetation fraction (e.g., larger than 50%); (2) a light saturation problem appeared in Figure 3.4a when the non-vegetation fraction was larger than 50%; (3) the light saturation problem disappeared if EANTLI was used instead of NTL (Figure 3.4b); (4) higher NTL values can be observed even for pixels with a very low non-vegetation fraction (e.g., less than 20%); (5) this problem was mitigated if EANTLI was used instead of NTL; (6) the EANTLI values at the 95th percentile line are in direct proportion to the non-vegetation fractions. The first finding indicates that the TMA method suffered from the problem of the mixture of ISA and bare land in a MODIS pixel. The second to fifth findings suggest the improvements obtained by using EANTLI instead of NTL. The sixth finding provides a hint as to how to build a relationship between ISA and EANTLI.

Generally, NTL should become brighter with the increase of the ISA percent (ISA%) because both the ISA and the NTL are good indicators of urbanization (Elvidge et al., 2007). From Figure 3.4, it can be seen that only the EANTLI values at the 95th percentile line can maintain the positive correlation of ISA% with NTL. In addition, the pixels with maximum EANTLI values in each non-vegetation fraction group should probably only include ISA as non-vegetation land cover (i.e., the non-vegetation fraction can be considered to be the ISA fraction for these pixels), whereas the pixels with smaller EANTLI values probably include both ISA and bare land as non-vegetation land cover. In this study, the EANTLI value at the 95th percentile line was used instead of the maximum EANTLI value in each group to build the relationship between ISA% and EANTLI. This was done for two reasons. First, the EANTLI values probably varied slightly even for the same ISA% (e.g., they varied from the 95th percentile line to the maximum). Second, the maximum EANTLI values were probably due to the imperfect removal of ephemeral lights from fires from those pixels (e.g., gas flares and forest fires, Elvidge et al., 2007). A sensitive test results shown in Figure 3.5 also indicate that the use of EANTLI values at the 95th percentile line is reasonable.

From Figure 3.5, it can be seen that the highest correlation coefficient and the smallest error index among the tested percentile lines occurred at 95th percentile except for a case of non-vegetation fraction less than 50% (occurred at 100th percentile line).

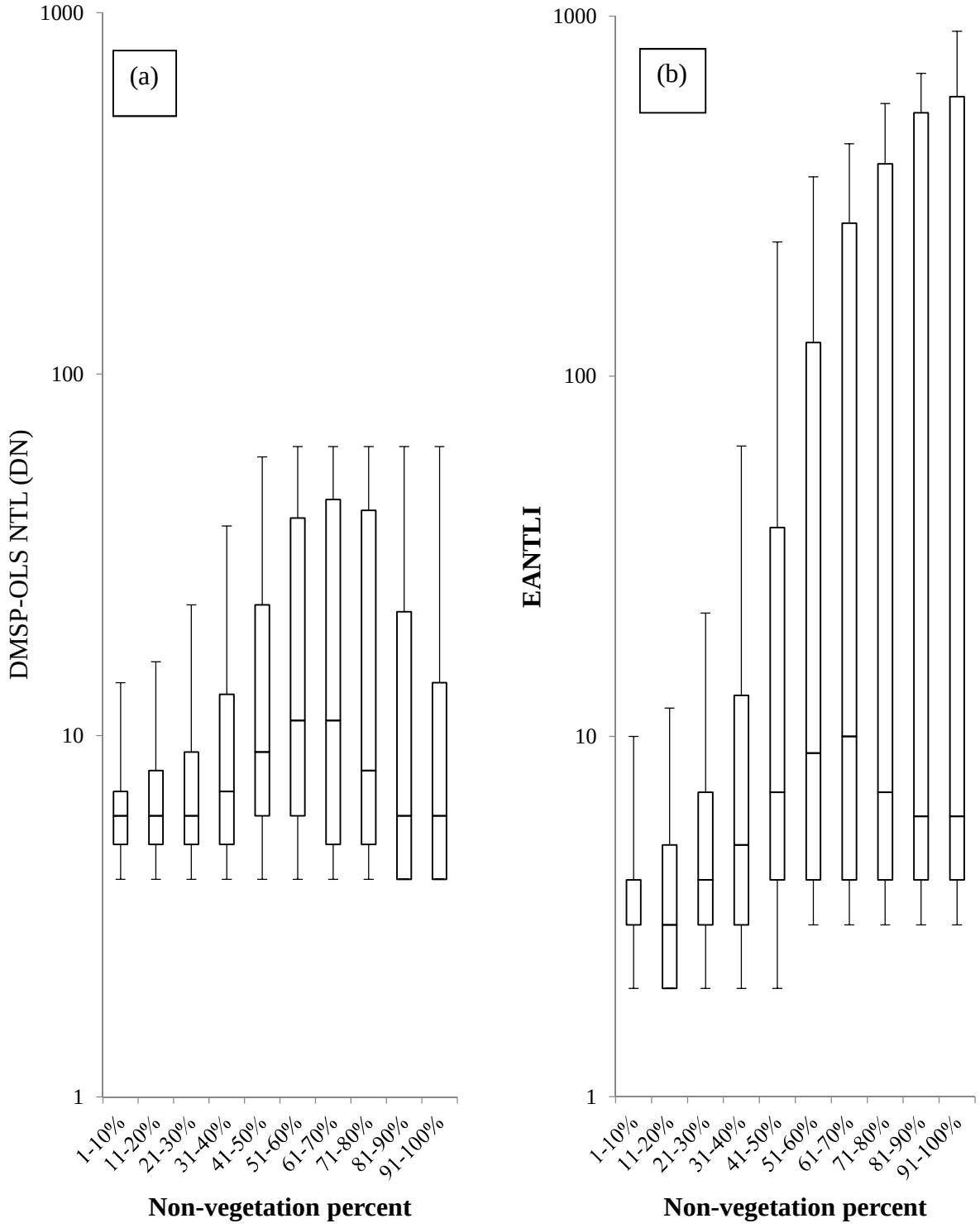

Figure 3. 4 Statistics of DN values of DMSP-OLS NTL (a) and EANTLI values (b) for 10 non-vegetation fraction groups ranging from 1% to 100% divided into deciles. For each group, the 5th, 25th, 50th, 75th and 95th percentiles are shown.

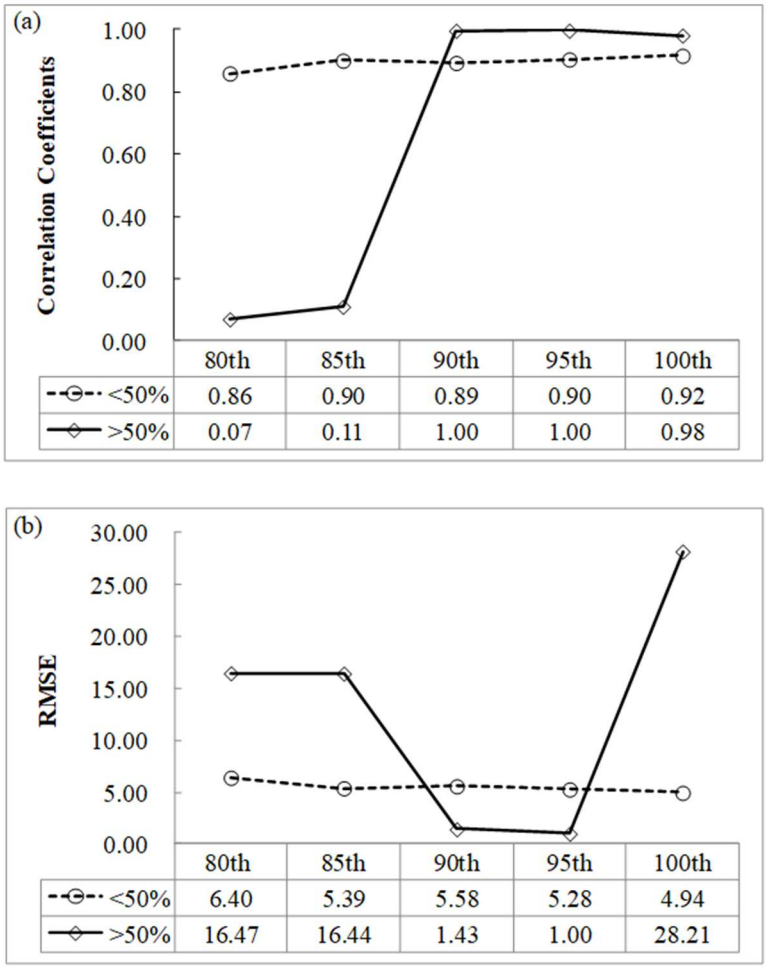

Figure 3. 5 Sensitivity of relationship between ISA% and EANTLI values to the use of EANTLI values at different percentile lines. a) Correlation coefficients between ISA% and EANTLI values at each tested percentile line. (b) Root mean square error (RMSE) of estimated ISA% using the relationship at each tested percentile line. <50%: the case for ISA% less than 50%; >50%: the case for ISA% larger than 50%.

Based on the above considerations, the scatter plots of the EANTLI values at the 95th percentile line and the corresponding ISA% values for each group are shown in Figure 3.6. It was found that the EANTLI values increased slowly with the ISA% values when the EANTLI values were less than 64 (corresponding to an ISA% value of 40%), but there appears to be a breakpoint at the EANTLI value of 236 (corresponding to an ISA% value of 50%) where the curve trend changed (i.e., above 236, the EANTLI values increased dramatically with the increase of ISA% values). This finding indicates that there exist two relationships between the EANTLI and ISA%

values. The first relationship can be represented by a natural logarithmic function for the EANTLI range between 0 and 236, and the second relationship can be represented by a polynomial function for EANTLI values larger than 236. The equations for the two relationships can be expressed as:

$$ISA\% = 8.5651 \times \ln(EANTLI) + 1.0063 \quad (EANTLI<236) \tag{4}$$

$$ISA\% = -0.00005(EANTLI)^2 + 0.1329(EANTLI) + 19.224 \quad (EANTLI \geq 236) \tag{5}$$

The constant term in Equation 5 was slightly adjusted from 20.464 to 19.224 to allow the two equations to give the same ISA% values at the breakpoint of EANTLI=236.

A preliminary ISA% map was then generated from the EANTLI image using Equations (4) and (5). The preliminary ISA% map was further compared to the non-vegetation fraction map, and the lower value was selected as the final ISA% value for each pixel. This is because non-vegetation land cover contains both ISA and bare land, and thus the ISA% should be equal to or smaller than the fraction of non-vegetation estimated using the TMA method.

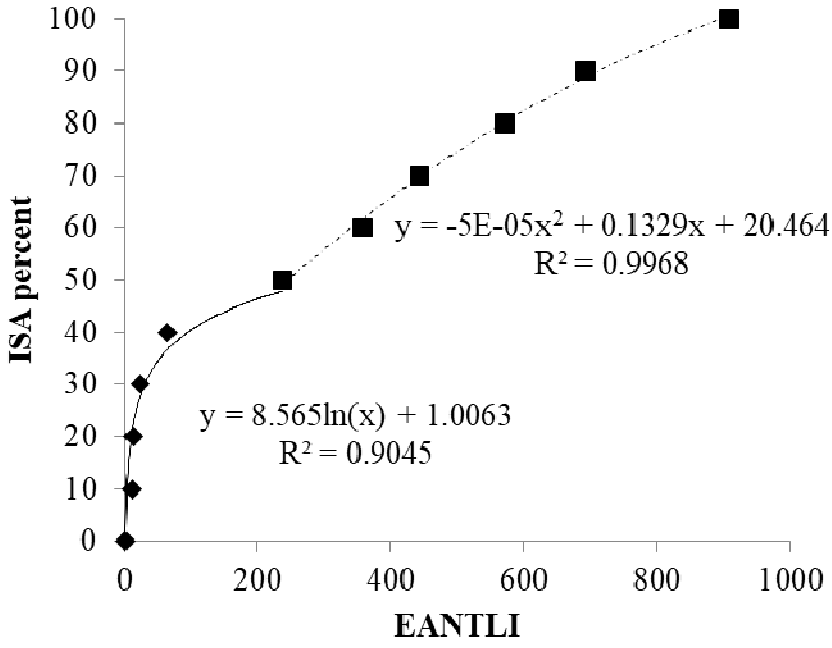

Figure 3. 6 Two relationships between the EANTLI and ISA% values.

3.3.4 Accuracy assessment

Two indices, namely the root mean square error (RMSE) and systematic error (SE), were used in accuracy assessment. These indices are defined as follows:

$$\mathrm{RMSE} = \sqrt{\frac{1}{n}\sum_{i=1}^{n}\left(\mathrm{ISA}_{\mathrm{est,i}} - \mathrm{ISA}_{\mathrm{ref,i}}\right)^2} \quad (6)$$

$$\mathrm{SE} = \frac{1}{n}\sum_{\mathrm{i}=1}^{\mathrm{n}}\left(\mathrm{ISA}_{\mathrm{est,i}} - \mathrm{ISA}_{\mathrm{ref,i}}\right) \quad (7)$$

where $\mathrm{ISA}_{\mathrm{est,i}}$ is the estimated fraction of the ISA from the MODIS and DMSP-OLS data, $\mathrm{ISA}_{\mathrm{ref,i}}$ is the referenced data in the sampling window *i*, and *n* is the total number of sampling windows for validation (a total of 97 samples were collected in this study). The RMSE denotes the sample standard deviation of the differences between the estimated values and the reference/observed values, while the SE denotes the average bias in the estimation. The coefficient of determination (R^2) between $\mathrm{ISA}_{\mathrm{est,i}}$ and $\mathrm{ISA}_{\mathrm{ref,i}}$ was also calculated.

3.4 Performance of the proposed method

Figure 3.7 shows the fraction map of non-vegetation based on the TMA method (Figure 3.7a), the preliminary fraction map of ISA obtained using Equations (4) and (5) (Figure 3.7b), and the final fraction map of ISA obtained through the selection of the smaller fraction values between the above two maps (Figure 3.7c). The EANTLI map is shown in Figure 3.7d for reference. From Figure 3.7a, it can be clearly seen that bare lands contributed quite a lot to the non-vegetation fraction, especially for the areas without any NTL (also see Figure 3.7d). The effects of bare lands on ISA estimation were greatly reduced through the combination of the non-vegetation fraction map and the EANTLI image (Figure 3.7b). These improvements occurred not only in areas without NTL (e.g., areas along the Mekong River denoted as Area 1 in Figure 3.7a; also see Figure 3.8a-c for a comparison of the details), but also in areas with NTL (e.g., the areas surrounding Bangkok,

Hanoi, Ho Chi Minh City, Vientiane, and Phnom Penh; also see Figure 3.8d-f for an enlargement of Area 2 in Figure 3.7a showing Phnom Penh city and its surrounding areas). Some slight changes were found when the final ISA fraction map (Figure 3.7c) was compared to the preliminary ISA fraction map (Figure 3.7b), such as in the areas in or surrounding Bangkok and Hanoi (also see Figure 3.8g-i for an enlargement of Area 3 in Figure 3.7a and also see the Google Earth image in Figure 3.8j for three special cases in Bangkok, which colors changed from yellow or red to green).

To quantitatively evaluate the performance of the proposed method, 97 samples (3 km × 3 km for each sample) from the historical images in Google Earth were interpreted and compared with the estimated ISA% values (Figure 3.9a). The corresponding 97 values for the non-vegetation fraction (TMA-based results, Yang et al., 2012) were also compared with the Google-Earth-image-based reference values for ISA% (Figure 3.9b). The RMSE of the proposed method was 0.111, with slight overestimation (SE = 0.061). In addition, 87% of the variance in the ISA% estimations determined by the proposed method corresponded with the estimations from Google Earth images ($R^2 = 0.87$). In contrast, the TMA-based results showed larger scatter (RMSE = 0.263) and overestimation (SE = 0.203), especially in low ISA% areas (i.e., less developed areas). The coefficient of determination was 0.58, which was also lower than that of the proposed method.

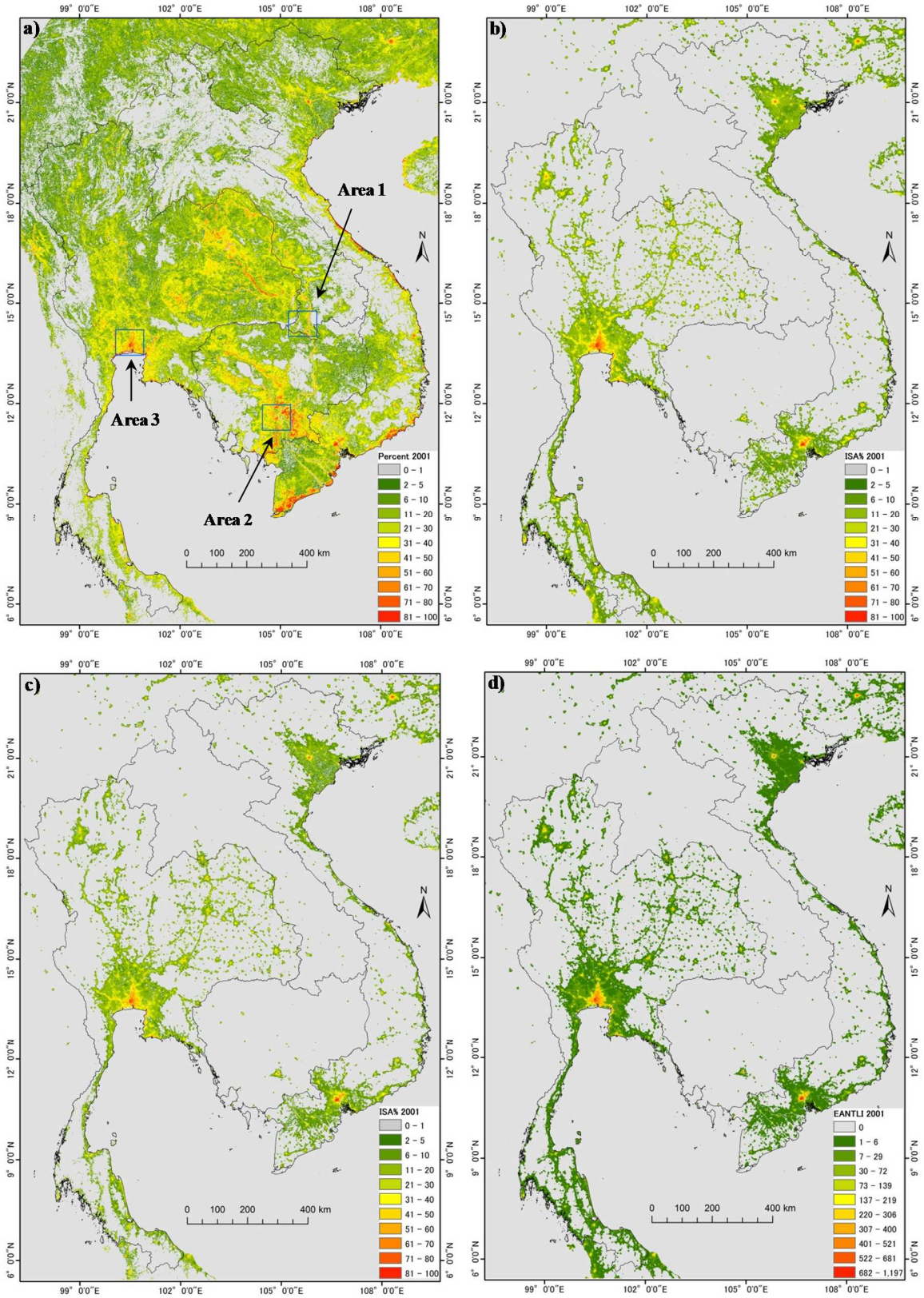

Figure 3. 7 Distribution maps of (a) non-vegetation fraction based on temporal mixture analysis method, (b) preliminary ISA fraction) and (c) final ISA fraction

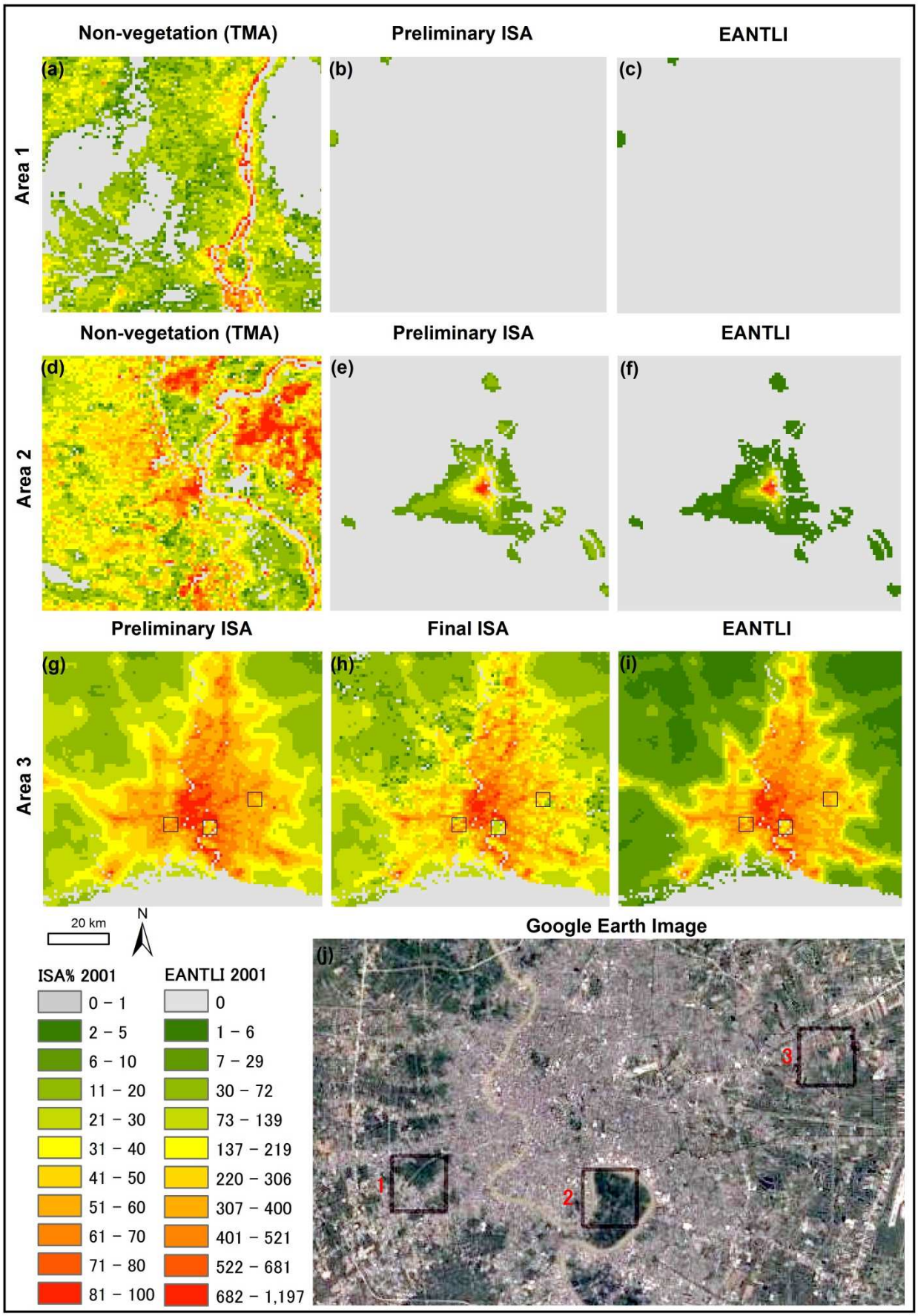

Figure 3. 8 Comparison of non-vegetation fraction map, preliminary ISA fraction map, final ISA fraction map, and EANTLI map for three example areas shown in Figure 3.7

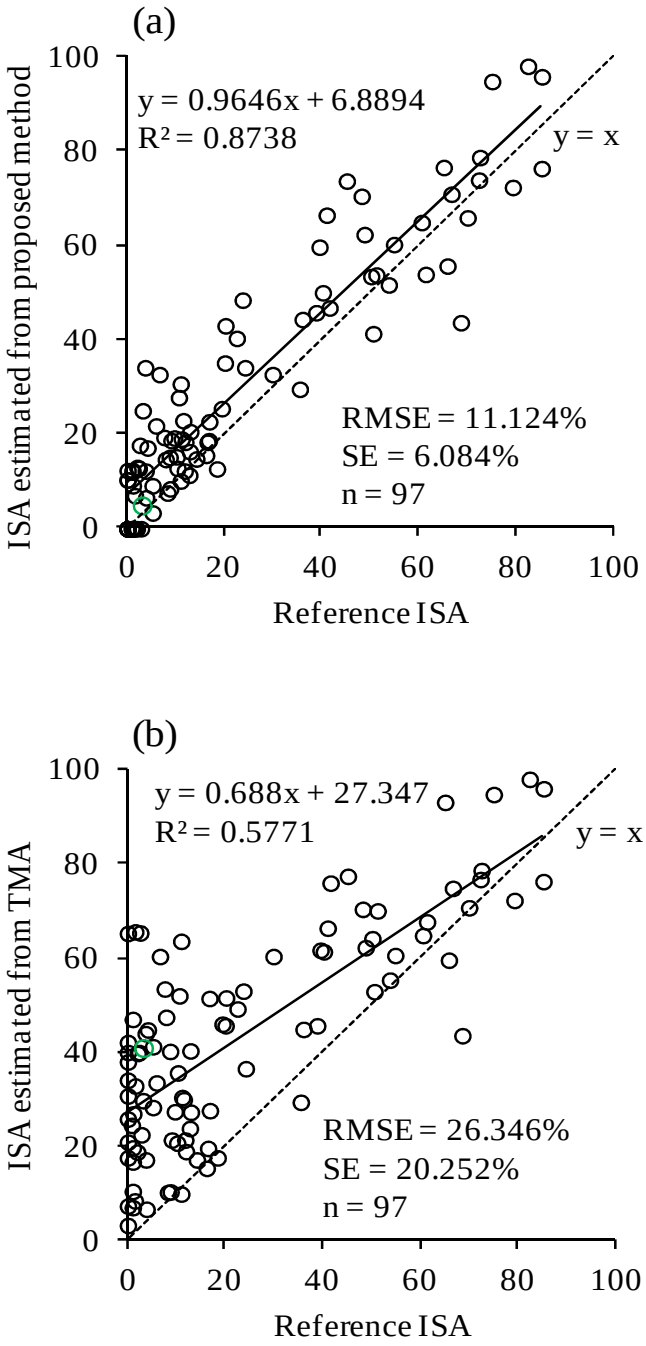

Figure 3. 9 Accuracy assessment. (a) Estimated ISA% by the proposed method are assessed by interpretation of the corresponding Google Earth images; (b) Estimated non-vegetation fraction based on TMA method are assessed by interpretation of the corresponding Google Earth images

Figure 3.10 provides a further demonstration of the proposed method using a selected sample from Figure 3.9 (green point). The Google Earth image was collected on February 12, 2001 from a rural area near Bangkok, Thailand (Figure 3.10a). From the Google Earth image, it can be seen that the major land use type of this sample is cropland with several small areas of ISA (e.g.,

some houses and roads, ISA% = 4.44% by visual interpretation). However, the TMA-based result showed a larger fraction of non-vegetation due to the presence of large amounts of bare land (Figure 3.10b, N-V% = 40.78%). Although the overestimation of ISA% from the TMA-based method was largely improved by the proposed method, a slight underestimation resulted because 5 of the 9 pixels had no lights but contained a small portion of ISA (gray pixels in Figure 3.10c, ISA% = 3.58%).

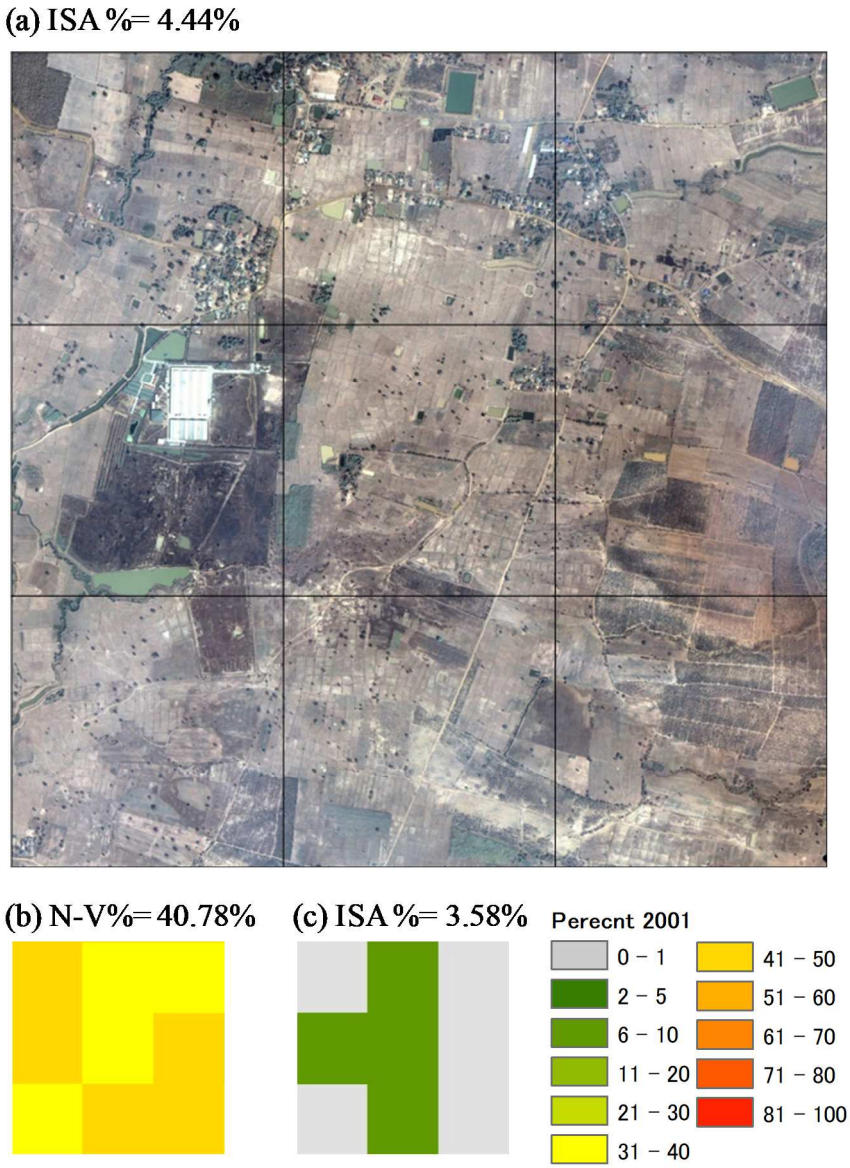

Figure 3. 10 Distribution maps for a selected sample (3 km by 3 km) from Figure 3.9 for visual comparison (a) reference image from Google Earth; (b) non-vegetation fraction (N-V%) estimated using the TMA method; (c) ISA% estimated using the method proposed in this study

3.5 Discussion

Building the relationship between ISA% and NTL is a key element in the proposed method. To do this, reference datasets of the ISA% and corresponding NTL values are necessary. Landsat TM/ETM + data have generally been used to generate a reference dataset of ISA% in previous studies (Elvidge et al., 2007; Lu et al., 2008; Liu et al., 2015; Huang et al., 2016). However, there are some drawbacks to the use of Landsat data for this purpose. First, the Landsat data still suffer from the mixed pixel problem in the ISA% estimation. Even though an SMA-based method was used to estimate ISA% from Landsat data, it remains a challenge to efficiently reduce endmember variability in the SMA-based method to provide a more accurate ISA% estimation due to the spectral complexity of each endmember (Yang et al., 2010; Somers et al., 2011). Second, additional time and labor are needed for processing Landsat data. This drawback will limit the application of this method for estimating ISA% on a large scale (e.g., regional or global). Furthermore, since Landsat data processing is time-consuming, it is not easy to frequently update a new regional or global ISA% product.

In this study, ISA% reference data were obtained by statistically analyzing the non-vegetation fraction and corresponding EANTLI data to avoid the need for Landsat data (Figure 3.4). The non-vegetation fractions were estimated from MODIS NDVI time-series data using the TMA method. The term “non-vegetation” was used in place of the term “ISA” in this step, because ISA and bare land have similar NDVI temporal profiles and thus can be considered the same endmember (Yang et al., 2014). It can be assumed that, in each non-vegetation fraction group, some pixels with the maximum EANTLI value only include ISA as the non-vegetation land cover (i.e., without bare land effects). According to this assumption, the non-vegetation fractions for these pixels can be considered ISA% reference data. The validation results shown in Figure 3.9 indicate that this assumption was reasonable in our study area. In addition, there are two advantages to using the TMA method instead of the SMA method for estimating the non-vegetation fraction: (1) the TMA method provides an efficient reduction of endmember variability;

and (2) this method is suitable for application on a large scale over a long term because it can be applied to MODIS time-series data (Yang et al., 2012).

For NTL, it is well known that two large obstacles (i.e., the light saturation problem and the blooming effects) have emerged in the application of the original DMSP-OLS data (Lu et al., 2008; Zhang et al., 2013; Zhuo et al., 2015). From Figure 3.4a, it can also be seen that the highest light intensities do not vary when the non-vegetation fraction is larger than 50%, and the higher light intensities are still found even when the non-vegetation fraction is smaller than 20%. These two problems can be solved through the use of the EANTLI image instead of the original DMSP-OLS image (Figure 3.4b). As mentioned in Section 3.3.3, the EANTLI values at the 95th percentile line were used in this study instead of the maximum EANTLI values. This led to 5% of the pixels in each non-vegetation fraction group with EANTLI values being larger than the EANTLI values used for building the relationships (i.e., Equations 4 and 5), and thus the ISA% values of these pixels in the preliminary ISA fraction map will be larger than the values of the corresponding non-vegetation fraction. In addition, imperfectly removed blooming effects can also cause overestimations in the preliminary ISA% map. These overestimations can be mitigated through the addition of the fourth step (e.g., Area 3 in Figure 3.7a–c; also Figure 3.8 g–j).

Lu et al. (2008) reported a natural-logarithmic-function-based regression model for estimating ISA% (i.e., referred to as “fractional settlements” in their paper) from the HSI values. However, the natural logarithmic function was only found to be suitable for the range of ISA% values between 0% and 50% in our study area (Figure 3.6). For ISA% values larger than 50%, the light intensities increased quickly with the increase of ISA%, and thus a quadratic-polynomial-function-based model was used to replace the natural-logarithmic-function-based regression model (Equation 5). These results probably indicate that different light use efficiencies existed between the developed and undeveloped regions in our study area.

Since global MODIS NDVI/EVI products are available for the year 2000 up to the present, a yearly non-vegetation fraction map can be generated on a global scale for the same period based

on the TMA method. On the other hand, yearly DMSP-OLS datasets are available from 1992 to 2013, and new NTL data (Suomi NPP-VIIRS: Suomi National Polar-Orbiting Partnership – Visible Infrared Imaging Radiometer Suite) have been collected since 2011. Therefore, it is possible to generate a yearly distribution map of ISA% values from 2000 to the present on a global scale using the proposed method. However, the size of the area that is the most appropriate for building the best relationship between ISA% and NTL should be further studied, for two reasons. First, the existence of a sufficient number of pixels with only ISA as a non-vegetation land cover is required for each of the 10 non-vegetation fraction groups (defined by deciles from 1% to 100%). Therefore, a larger area is necessary to meet this requirement. Second, the light use efficiency probably differs among countries or regions of the world due to different levels of economic development. Therefore, it is better to use different relationships to obtain more accurate ISA% estimations for each country or region, and thus a smaller study area should be selected. These two considerations are contradictory. In addition, although the MODIS NDVI/EVI products are only available from year 2000, the NDVI time-series data can be extended to the 1980s by using the data from the Advanced Very High Resolution Radiometer of the NOAA (NOAA/AVHRR). Therefore, it is possible to obtain a global ISA% map since 1992 if the NDVI is used to replace EVI in Equation 3. However, how the replacement influences the performance of NTL data should be further investigated in a future study. Moreover, inter-annual correction should also be implemented to reduce temporal inconsistency between spatially enhanced DMSP-OLS NTL time-series data (i.e., EANTLI in this study, Xie and Weng, 2017).

3.6 Conclusions

In this study, an easily implemented method was developed for estimating ISA% on a large scale. The developed method includes four major steps and requires three major products from two satellite sensors. The four major steps are: (1) estimate the non-vegetation fraction from MODIS NDVI time-series products using the TMA method; (2) obtain improved NTL data by

calculating EANTLI from the monthly MODIS EVI product and DMSP-OLS NTL data; (3) generate a preliminary ISA% map by building a relationship between ISA% and EANTLI based on the statistical analysis of the maps from the first and second steps; (4) obtain a final ISA% map by comparing the preliminary ISA% map to the non-vegetation fraction map and selecting the smaller values. The validation result showed that the developed method has promising accuracy for estimating the ISA% in our study area (which mainly consists of four Southeast Asian countries: Thailand, Laos, Cambodia, and Vietnam), with an RMSE value of 0.111, an SE value of 0.061, and a determination coefficient of 0.87. Another important finding is that there are two relationships between ISA% and the improved NTL (i.e., EANTLI): the natural logarithmic function is suitable for ISA% values between 0 and 50%, and the quadratic polynomial function should be used for ISA% values larger than 50%. The developed method shows high potential for use in generating a global ISA% map with frequent updates because of its easy implementation and readily available input data.

Chapter 4

Impervious cover change in the lower Mekong region from 2001 to 2012 and the impacts on drainage basins

4.1 Introduction

Urbanization, a phenomenon that involves changes in demographics, economy and land cover (Zhang and Seto, 2011), has led to an increase in the amount of impervious surfaces. These surfaces, such as buildings, roads, sidewalks and parking lots prevent rainwater from infiltrating into the soil. The impervious surfaces have been known to have a negative impact on the environment of drainage basins and water quality (Alberti et al., 2007; Shuster et al., 2005; Theobald et al., 2009; Liu et al., 2013; Kim et al., 2016). Increases of impervious surface area (ISA) can alter ecological, hydrological and thermal characteristics of a drainage basin or watershed. Increased ISA during the urbanization or development process also means a loss of natural land covers such as vegetation and bare soil, which can enhance surface temperature changes and urban heat island (Grimm et al., 2008; Buyantuyev and Wu, 2010; Li et al., 2011). ISA contributes to the hydrological changes that degrade water quality (Klein, 1979; Jacobson, 2011). As the ISA increases, the infiltration of rainwater decreases and the speed and volume of surface runoff increase, which consequently can cause flooding and bank erosion. In addition, increased runoffs due to ISA can transport nonpoint-source pollutants directly into waterbodies. The decreased penetration of rainwater reduces groundwater recharge and lowers water tables, which threatens water supplies for humans and reduces the groundwater contribution to stream flow (Arnold & Gibbons, 1996). Impervious surfaces also alter the ecological conditions in a drainage basin. As increased ISA causes a reduction in natural land cover as well as alterations of hydrological and thermal characteristics in watersheds, the biodiversity and ecosystem are affected (Bierwagen et al., 2010; Matsushita et al., 2014).

Percentage of ISA in a watershed is strongly related to watershed health and water quality (Schueler, 2009). It has been widely accepted that a drainage basin or watershed can be classified into four categories according to the percentage of ISA relative to the total area of drainage basins. A basin is considered as having normal function or "no_impact" if the percentage of ISA is less than 1%, "stressed" if the percentage of ISA is between 1% and 10%), "impacted" if the percentage of ISA is between >10% and 25%, and "degraded" if percentage of ISA is larger than 25% (Schueler, 1994; Arnold & Gibbon, 1996; Bierwagen et al., 2010). Identifying the impact categories of drainage basins from the amount of ISA is critical for watershed managers and policy makers. Understanding where and which basins are not affected, stressed, impacted or degraded helps to timely and better manage and regulate the impervious cover growth to protect the drainage basin quality.

Southeast Asia has experienced rapid economic development and population growth. Consequently, a lot of infrastructure, buildings, and other impervious surfaces have been built and urban area has been significantly expanded, especially over the past several decades. In the four countries located downstream of the Mekong River (Laos, Thailand, Cambodia and Vietnam), there is a lack of studies on changes of drainage basins' health in relation to percentage of ISA due to limited availability of large-scale ISA maps from different periods. The global ISA is only available for 2000-2001 (Elvidge et al., 2007), and there is no update since then. Yang et al. (2010) mapped ISA for Lake Kasumigaura basin for 1987, 2000 and 2007 from Landsat images and analyzed the impacts on the basin, revealing that the basin were in the impacted category and will be in the degraded category in 2017. The study was at a basin scale and only three single time periods. Kuang et al. (2013) produced ISA maps for 2000 and 2008 to assess the impact on watersheds in China. A method to estimate ISA in the lower Mekong region using MODIS and DMSP-OLS NTL data was developed in Chapter 3. The strength of this method is that is can easily map ISA on a yearly basis due to the availability of the satellite data, and therefore it is possible to more frequently monitor the status of watersheds. The objectives of this chapter were: 1) to

generate annual ISA distribution maps for the lower Mekong region from 2001 to 2012 using the developed method and evaluate its applicability; and 2) to analyze ISA changes at different spatial scales as well as the ISA impacts on drainage basins containing in the region. The study was focused the ISA change from 2001 to 2012 because the region has witnessed significant economic and population growth.

4.2 Datasets

In this study, MODIS NDVI (MOD13A2 product), MODIS EVI (MOD13A3 product), MODIS Land Water mask (MOD44W product) and DMSP-OLS nighttime lights (NTL) data from 2001 to 2012 were used. The three MODIS products were downloaded from NASA website through online Reverb tool (https://reverb.echo.nasa.gov/reverb/). MOD13A2 product is a 16-day composite and MOD13A3 is a monthly composite of the highest quality pixels from daily images. These two products have a spatial resolution of 1000 m. Six MODIS tiles (h27v6, h27v7, h27v8, h28v6, h28v7, h28v8) were required to cover the study area (Figure 2.1). MODIS NDVI time-series (23 composites per year), and MODIS EVI time-series (12 composites per year) from MOD13A3 spanning twelve years from 2001 to 2012 were used in this study. MODIS Land-Water mask with 250 m spatial resolution, which subsequently was resampled to 1000 m, was used to mask water pixels from the images. All the MODIS data were reprojected from their original Sinusoidal projection to Albers Equal Area Conic projection and subsetted to the study area.

DMSP-OLS NTL data used in this study were the stable lights from 2001 to 2012 (F152001, F152002, F152003, F152004, F152005, F152006, F152007, F162008, F162009, F182010, F182011, and F182012) included in the Version 4 DMSP-OLS NTL Time Series. The DMSP-OLS NTL data were processed and archived by NOAA's National Geophysical Data Center (https://www.ngdc.noaa.gov/eog/index.html). The stable lights are annual composites made by averaging all the available NTL images. Prior to compositing, the images are filtered to exclude

clouds, auroras, moonlight, sunlight and solar glare. It is estimated that each pixel in the annual composites is the product of 20 to 100 clear observations (Elvidg et al., 2009). The stable lights contain lights from cities, towns, and other sites with persistent lighting, including gas flares, with ephemeral events, such as fires removed. The data have a spatial resolution of 1000 m and are a 6-bit integer whose digital number (DN) values range from 0 to 63, with zero being the background noise and 63 being the maximum light intensity. The NTL data were reprojected from Geographic projection to Albers Equal Area Conic projection and subsetted to the same extent as MODIS data described above.

The shapefile of drainage basin boundary was derived from the National Institute for Environmental Study, Japan (http://www.cger.nies.go.jp/db/gdbd/gdbd_index_e.html). There are a total of 847 drainage basins that are completely within the study area.

4.3 Methods

4.3.1 Data pre-processing

For the MODIS NDVI temporal profiles, a smoothing method based on Savitzky-Golay filter (Chen et al., 2004) was applied. The purpose of this filter was to minimize the remaining cloud and/or noise contamination in the images. According to previous researches (Yang et al., 2012; Yang et al., 2014), accuracy of ISA estimation has been improved when using the sorted NDVI temporal profiles at higher section due to reduction in variability within an endmember class. Therefore, the filtered NDVI temporal profiles were then rearranged in ascending order, and only the last twelve highest NDVI elements were finally extracted for utilizing in the TMA. For MODIS EVI data, the downloaded monthly composites were combined to produce annual composites which were one of the inputs for computing EVI-Adjusted Nighttime Light Index (EANTLI) (Zhuo et al., 2015).

Comparability and consistency of DMSP-OLS NTL images from different years and different satellites should be taken into account before using them for any change analysis. It is known that there is no onboard calibration in the OLS sensors (Elvidge et al., 2009). In addition, undocumented gain adjustment, sensor degradation, satellite shift and atmospheric effects are also considered as the reasons why the sensors produced different DN values for the same ground feature (Cauwels et al., 2014; Zhang et al., 2016; Huang et al., 2016). Thus, inter-calibration of the time-series NTL datasets from OLS sensors is required to improve the temporal consistency and comparability. As reviewed by Pandey et al., 2017, a number of studies have proposed the methods for inter-calibration of stable NTL images (annual composites) on regional or global scales (e.g. Elvidge et al., 2009; Small & Elvidge 2013; Elvidge et al., 2014; Bennie et al., 2014; Zhang et al., 2016; Li and Zhou, 2017). In the present study, inter-calibration of the NTL time-series was carried out by using the stepwise calibration method, most recently proposed by Li and Zhou (2017). The stepwise method could address the difficulties in selecting invariant region and appropriate year as reference image and over modification in the previous studies (e.g. Elvidge et al., 2014 and Zhang et al., 2016). The stepwise method calibrated all the stable NTL images collected from six satellites (F10, F12, F14, F15, F16, and F18) from 1992 to 2013. The key improvements in this method are: systematic correction of the NTL images for each satellite instead of the entire NTL time-series, and use of the temporally neighbored image as a reference for calibration. Therefore, it minimally modified the raw NTL images while produced a more consistent NTL time-series which was indicated by a smoother increasing trend of sum of NTL. In this present study, only the NTL images from 2001 to 2012 were used for estimating ISA.

Further correction was implemented to the calibrated NTL images because through examination of each image it was found that the same pixels are lit (DN value > 0) in some years but non-lit (DN value = 0) in some other years. Moreover, the number pixels of NTL images were not temporally consistent with abnormal changes between 2006 and 2012 (Figure 4.1).To ensure that the ISA dynamics reflect the actual urbanization process in the study area over the period, we

assumed that NTL detected in the previous year would not disappear in the following years. Based on this assumption, the calibrated NTL images from 2001 to 2012 was adjusted so that the non-lit pixels in the later year were replaced by the lit pixels in the earlier year. In the adjustment process, we used NTL image in 2000 as the starting image, the adjusted NTL image in 2001 as the next, and so forth:

$$DN_{(n)} = \begin{cases} DN_{(n)} & \text{if } DN_{(n)} > 0 \\ DN_{(n-1)} & \text{if } DN_{(n)} = 0 \text{ and } DN_{(n-1)} > 0 \\ 0 & \text{Otherwise} \end{cases} \quad (8)$$

where n represents the year (2001, 2002,…,2012); $DN_{(n)}$ and $DN_{(n-1)}$ are the DN values of the NTL images in n^{th} and $(n-1)^{th}$ years respectively.

The temporal consistency of the DMSP-OLS NTL data from 2001 to 2012 has improved after performing inter-calibration and further correction (Figure 4.1). The number of pixels of the original NTL image was the same as those of the inter-calibrated NTL image for each year. However, the number of pixels increased through time after further correction using the assumption that lit pixels in the previous year should not disappear in the later years. Sum of lights (i.e. the sum of all lit pixel values in the image) is an indicator of the NTL temporal consistency. According to Figure 4.1b, it can be clearly seen that after intercalibration the NTL time series (2003 to 2007) with low sum of lights was improved. In addition, the sum of lights increased temporally from 2003 to 2006, then leveled before it slightly dropped in 2009. Remarkably, there was a sudden rise from 2009 to 2010. After further correction, the fluctuations were all removed, and the sum of lights has increased steadily from 2001 to 2012. For each individual country in the study area the improvement in consistency of DMSP-OLS NTL time-series was also seen (Figure 4.2). Similar to the whole region, for each country the NTL time-series was originally not consistent, but has improved after inter-calibration and further correction using the assumption that NTL detected in the previous year do not disappear in the following years.

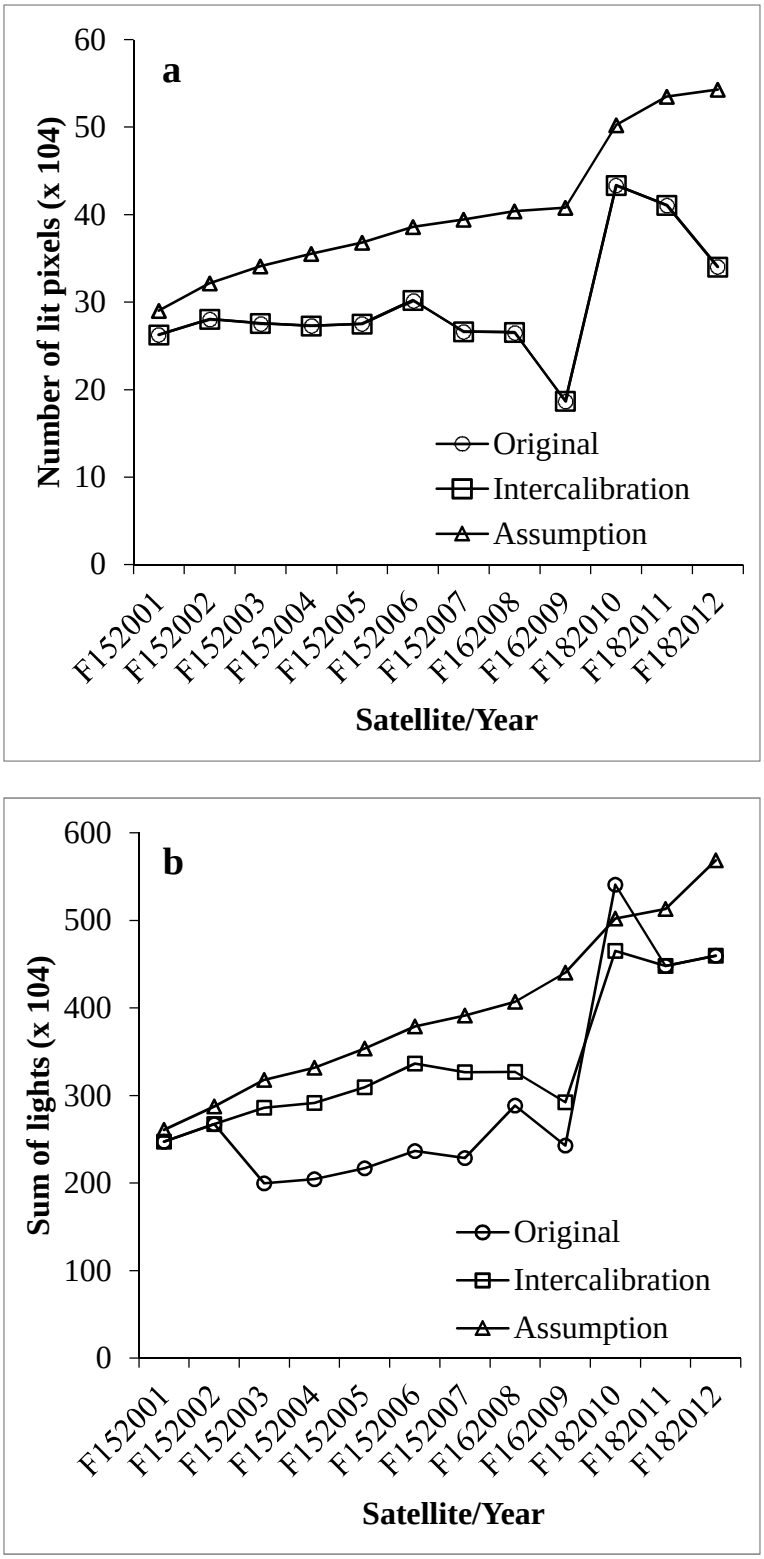

Figure 4. 1 Total number of lit pixels (a) and sum of lights (b) from the original, inter-calibrated and further corrected NTL data for the lower Mekong region from 2001 to 2012

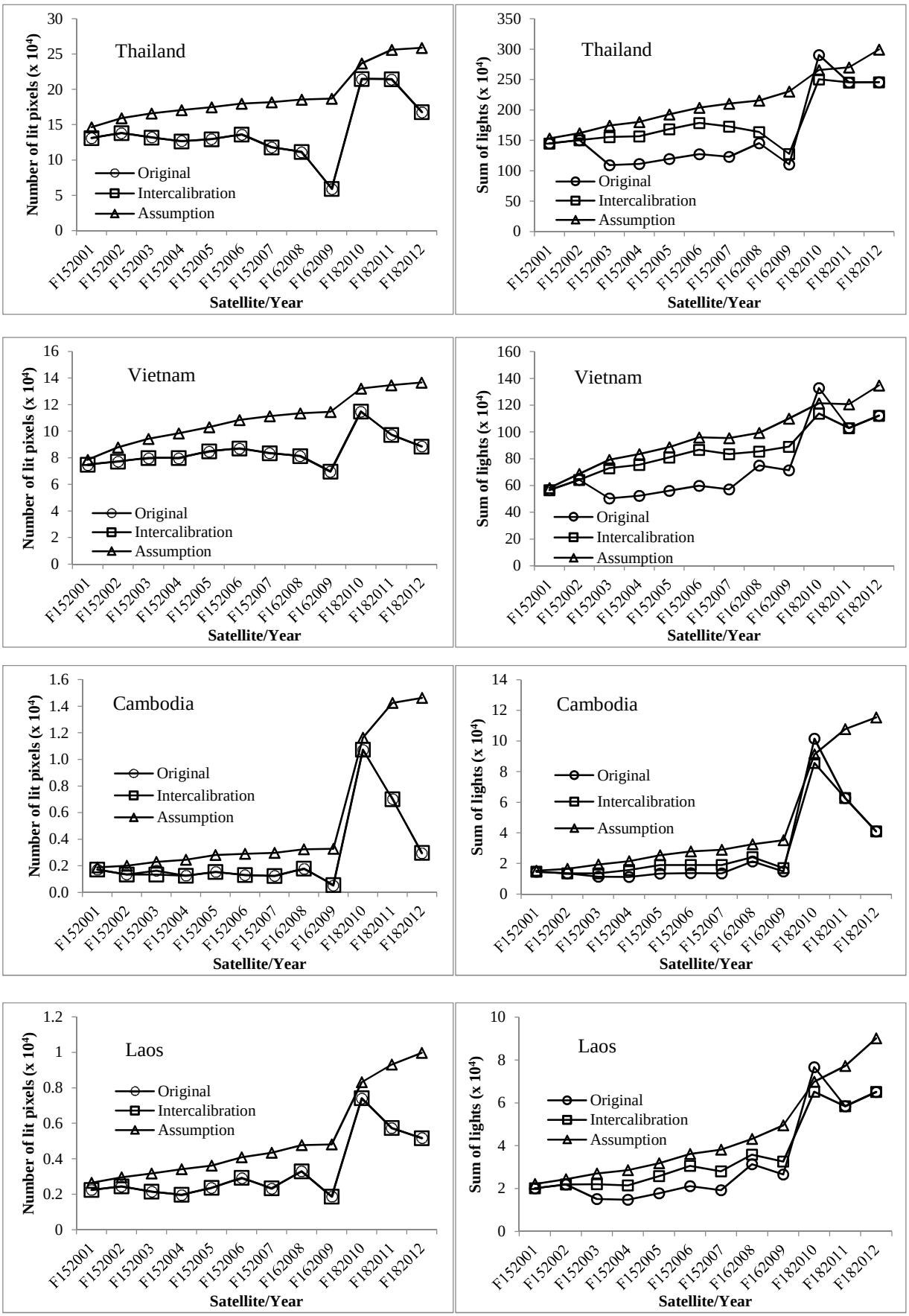

Figure 4. 2 Total number of lit pixels and sum of lights from the original, inter-calibrated and further corrected NTL data for the each country in the study area from 2001 to 2012.

4.3.2 Estimating ISA from 2001 to 2012

ISA for each year from 2001 to 2012 was estimated from MODIS and DMSP-OLS NTL data following the method developed in Chapter 3 above. The method consists of four main steps. First, the non-vegetation fraction is estimated from MODIS NDVI time-series using the TMA approach. Second, an improved nighttime light called EANTLI is computed from MODIS EVI and DMSP-OLS NTL data. Third, a preliminary ISA% map is generated by constructing a relationship between ISA% and EANTLI based on the statistical analysis of the non-vegetation fraction and preliminary ISA% maps. Fourth, a final ISA% map is obtained by comparing the preliminary ISA% map to the non-vegetation fraction map and choosing the smaller values.

The method is appropriate for estimating ISA over a large area, such as the lower Mekong region. In addition, building a relationship between ISA% and EANTLI is the key element in the method. To build the relationship, previous studies generally estimated reference ISA data from Landsat or higher resolution satellite images, which requires much time and labor and makes it very difficult to produce ISA maps for other years. Instead, this method took advantages of non-vegetation fraction map estimated from MODIS NDVI time-series data using TMA. As the non-vegetation fraction includes ISA and/or bare land, it is possible to identified pixels that contain only ISA fraction through statistical analysis. From these ISA values and the corresponding EANTLI values, the relationships were generated.

4.3.3 Extracting ISA for each drainage basin in the study area

The amount of ISA in each drainage basin was extracted from the ISA maps from 2001 to 2012 produced in this study by using the shapefile of drainage basin boundary. In addition, the percentage of ISA in each of the drainage basins (the ratio of total ISA to the drainage basin area) was calculated. Previous studies have demonstrated the strong correlation between the percentage

of ISA in a watershed and the watershed quality (Klein 1979; Schueler, 1994; Arnold and Gibbons, 1996; Bierwagen et al., 2010). Although there were slight differences in the determination of watershed categories in these studies, in general four categories of watershed can be classified based on the percentage of ISA in each watershed. These four categories are: "no_impact" (percentage of ISA less than 1%), "stressed" (percentage of ISA between 1% and 10%), "impacted" (percentage of ISA between >10% and 25%) and "degraded" (percentage of ISA greater than 25%). The watersheds or basins within no_impact category have normal function and no effect on aquatic system. The basins in stressed category still function normally with almost no effect, and are the most protective in which ISA control or strict measures should be done to maintain predevelopment basin quality. The basins in impacted category potentially start to degrade and experience some loss of biodiversity. The basins in degraded category stop functioning, in which water quality and biodiversity became fair or poor. In this study, a total of 847 drainage basins for each year were classified into these four categories.

4.4 Results

4.4.1 Annual ISA maps between 2001 and 2012

The relationships between ISA% and EANTLI with the determination coefficients (R^2) for each year from 2001 to 2012 are presented in Table 2 and the corresponding graphs are shown in Figure 4.3. It was found that like the results in Chapter 3, the two relationships of natural logarithmic function (for ISA% less than 50%) and second order polynomial function (for ISA% greater than or equal 50%) existed for all the years. Overall, the equations for the twelve years have very good fit with R^2 for all the natural logarithm functions being higher than 0.90, and for all the second order polynomial functions being higher than 0.98. The relationships were similar for all the years, with no significant differences. In addition, the EANTLI values at the break points of the two relationship range from the lowest of 176 (in 2010) to the highest of 239 (in 2012).

These implies that the relationships should be built year by year. Figure 4.4 shows the ISA distribution maps from 2001 to 2012 produced in this present study. A visual examination of the twelve maps show a general growth of ISA amount from year to year. More detailed analyses are described in the following section.

Table 2 Relationships between ISA and EANTL for each year from 2001 to 2012

Year	EANTL < b	R^2	EANTLI >= b	R^2	b
2001	ISA% = 8.7282×ln(EANTL) + 2.0981	0.9502	ISA%= -1E-04(EANTLI)^2 + 0.1911(EANTLI) + 13.5854	0.9971	205
2002	ISA% = 8.9143×ln(EANTL) + 2.6537	0.9587	ISA% = -7E-05(EANTLI)^2 + 0.1802(EANTLI) + 17.7162	0.997	190
2003	ISA% = 8.7143×ln(EANTL) + 1.4044	0.9519	ISA% = -8E-05(EANTLI)^2 + 0.1794(EANTLI) + 14.3757	0.9982	205
2004	ISA% = 8.5193×ln(EANTL) + 0.9785	0.9446	ISA% = 1E-04(EANTLI)^2 + 0.0752(EANTLI) + 25.5444	0.9982	220
2005	ISA% = 8.7256×ln(EANTL) + 1.1191	0.9401	ISA% = 1E-05(EANTLI)^2 + 0.1171(EANTLI) + 23.4525	0.9972	201
2006	ISA% = 8.7120×ln(EANTL) + 1.3335	0.9521	ISA% = 1E-04(EANTLI)^2 + 0.0554(EANTLI) + 32.4641	0.9891	199
2007	ISA% = 8.6672×ln(EANTL) + 0.5327	0.9265	ISA% = -5E-05(EANTLI)^2 + 0.1576(EANTLI) + 17.5911	0.9996	193
2008	ISA% = 8.6534×ln(EANTL) + 0.535	0.9269	ISA% = -9E-05(EANTLI)^2 + 0.1936(EANTLI) + 12.0628	0.9983	193
2009	ISA% = 8.2549×ln(EANTL) - 0.3453	0.9001	ISA% = 4E-05(EANTLI)^2 + 0.1211(EANTLI) + 15.1939	0.9981	224
2010	ISA% = 8.8797×ln(EANTL) + 0.7563	0.9300	ISA% = 3E-05(EANTLI)^2 + 0.1101(EANTLI) + 26.3618	0.9972	176
2011	ISA% = 8.6311×ln(EANTL) + 1.1119	0.9429	ISA% = -3E-05(EANTLI)^2 + 0.1409(EANTLI) + 19.345	0.9974	206
2012	ISA% = 8.2438×ln(EANTL) + 0.2073	0.9266	ISA% = -5E-05(EANTLI)^2 + 0.1767(EANTLI) + 5.9789	0.9978	239

Note: b is the EANTLI value at the breakpoint between the two relationships.

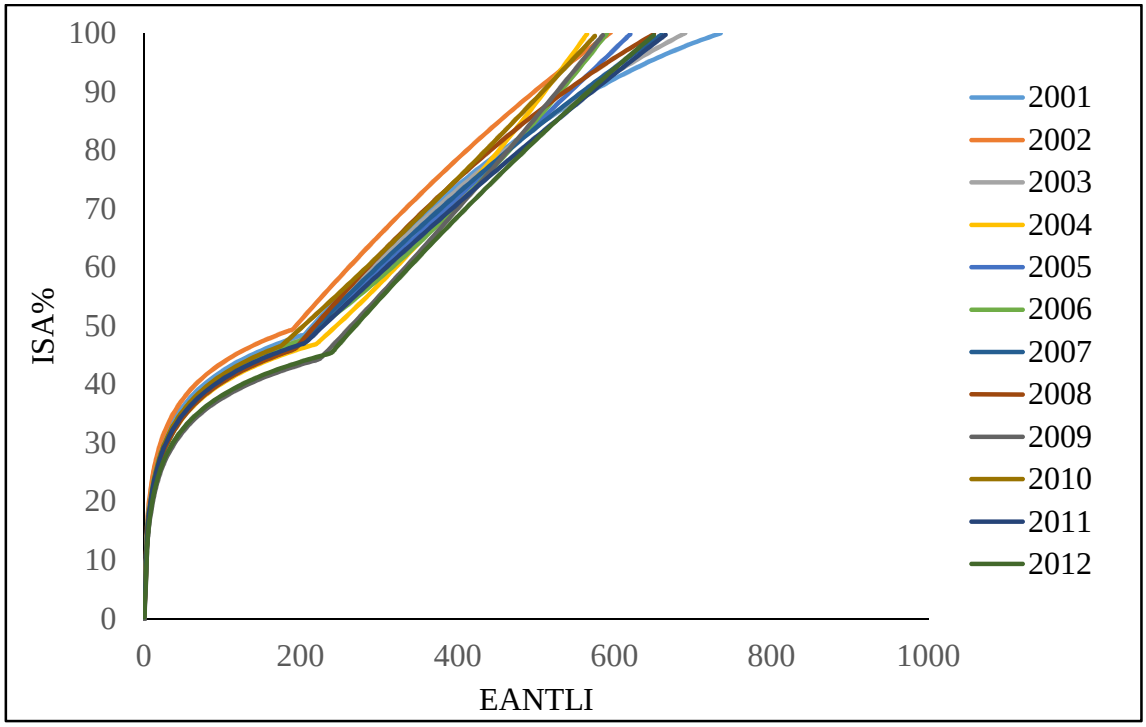

Figure 4. 3 The two relationships between ISA% and EANTLI for each year

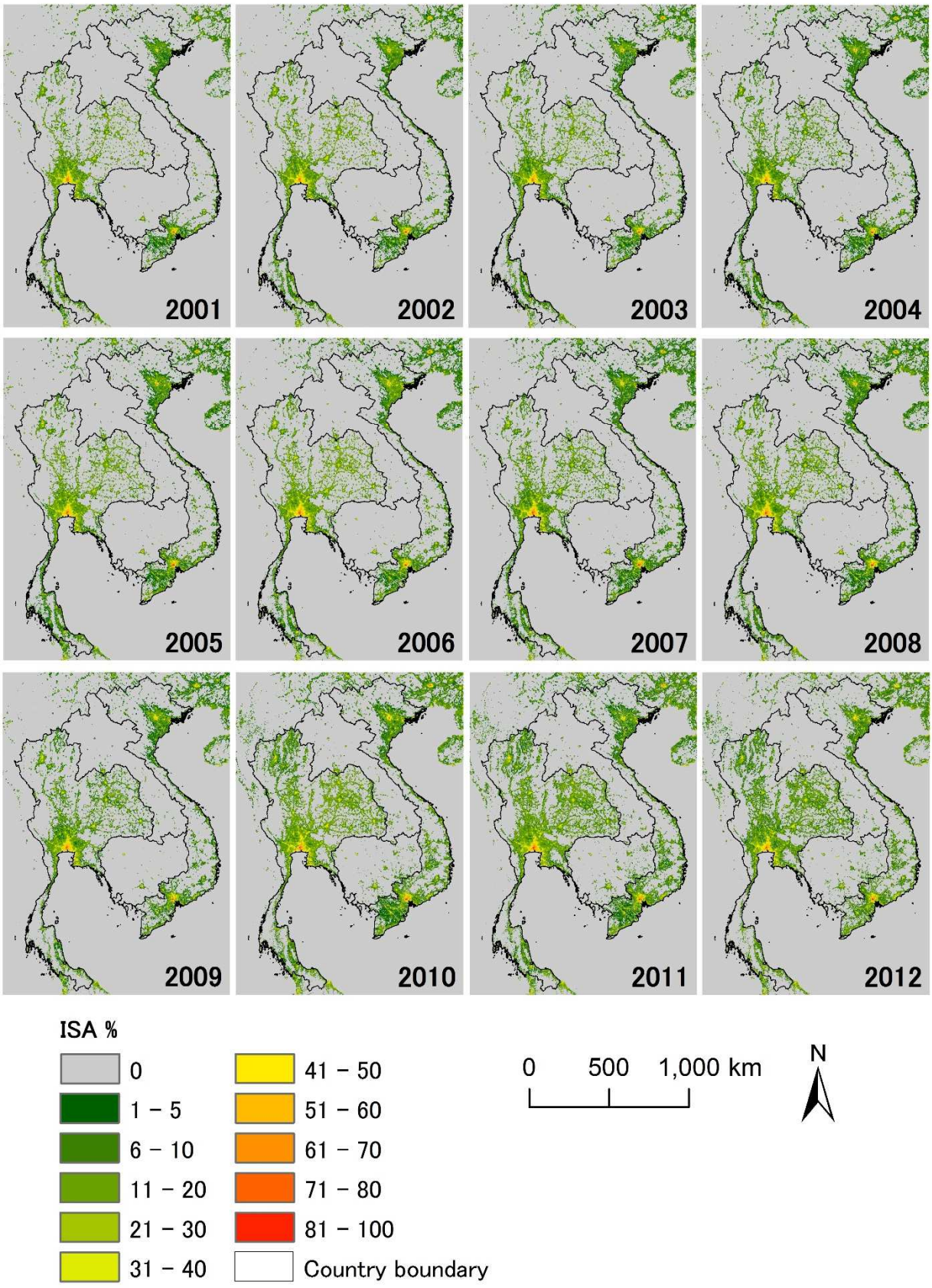

Figure 4. 4 ISA maps of the lower Mekong region from 2001 to 2012.

4.4.2 ISA change at regional and country level from 2001 to 2012

Figure 4.5 shows the amounts of estimated ISA for the lower Mekong region from 2001 to 2012. There was an increasing trend over the period (R^2 = 0.76). The analysis revealed that the region had a significant ISA increase by 62 percent from 29,398 km^2 (1.73% of the total land area) in 2001 to 47,635 km^2 (2.81%) in 2012. The annual increase was estimated by using linear regression model of all the 12 years' ISA data at 1803 km^2 per year. This indicates rapid urban growth and loss of other land covers such as agricultural land over the eleven-year period.

All of the four countries within the lower Mekong region had an increasing trend in ISA (Figure 4.6). Overall, the R^2 is higher than 0.67 for all the countries. In addition, it can be seen that Thailand had the largest share of ISA, followed by Vietnam, Cambodia and Laos. In 2012, Thailand had ISA of 25,110 km^2 (4.88% of Thailand's land area), Vietnam 12,055 km^2 (3.67% of Vietnam's land area), Cambodia 1,143 km^2 (0.63% of Cambodia's land area) and Laos 855 km^2 (0.37% of Laos's land area). Using the linear regression models of the ISA data over the twelve years for each country, the average annual increases of ISA were estimated at 56 km^2/year, 89 km^2/year, 442 km^2/year and 829 km^2/year for Laos, Cambodia, Vietnam and Thailand respectively. The ISA in Thailand and Vietnam increased steadily, while the ISA in Laos and Cambodia increased exponentially over the eleven-year period. The remarkable increase in the amount of ISA in Thailand and Vietnam was probably due to the construction of physical infrastructure, buildings, factories, etc. to meet the fast growing economy and rising population during the period (see Figure 2.2). However, surprisingly despite smaller population than Vietnam, Thailand had a larger amount of ISA than Vietnam. For Laos, the amount ISA increased slowly from 283 km^2 (0.12% of its country's land area) in 2001 to 461 km^2 (0.20%) in 2009 and soared to about 898 km^2 (0.39%) in 2011. Similarly, for Cambodia the amount of ISA slowly rose from 213 km^2 (0.12% of its country's land area) in 2001 to 375 km^2 (0.20%) in 2009, and then rocketed to 1,232 km^2 (0.67%) in 2011.

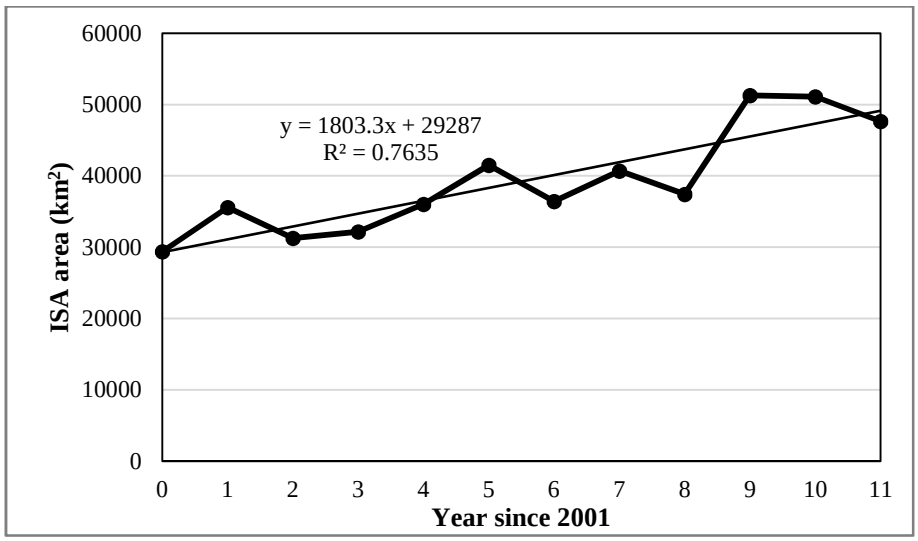

Figure 4. 5 ISA change for the lower Mekong region.

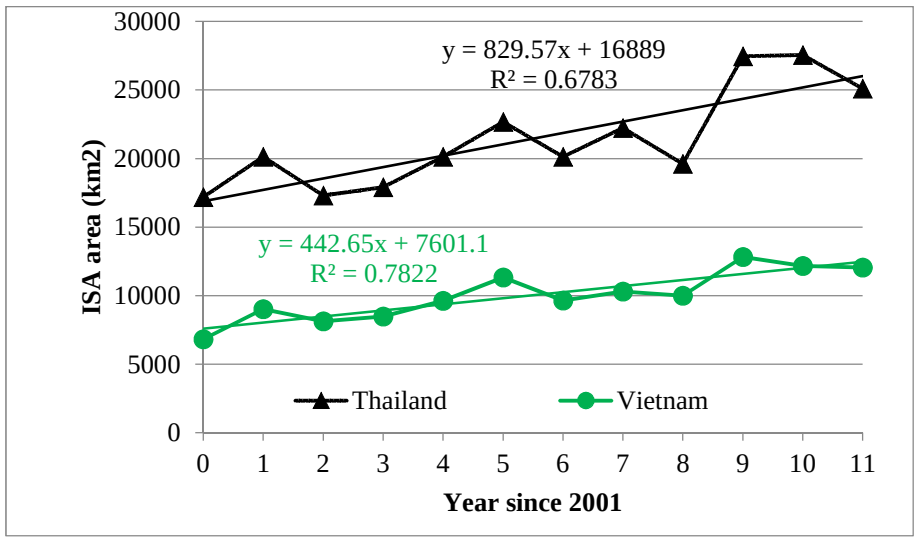

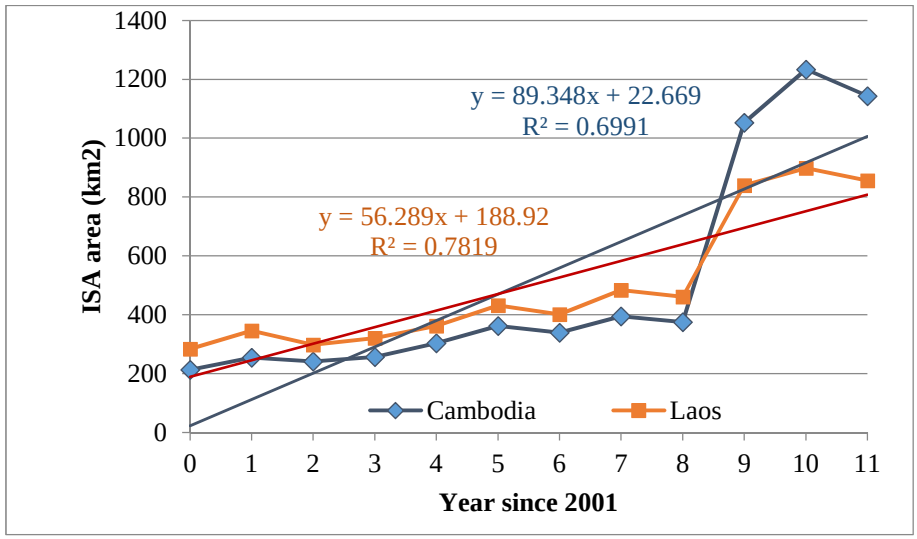

Figure 4. 6 ISA change for each country of the lower Mekong region.

4.4.3 Impacts of ISA on drainage basins in the lower Mekong region (2001-2012)

Figures 4.7 and 4.8 provide data on the number of drainage basins classified by the ISA impacts. Of a total of 847 drainage basins, there were 524 (61.9%) in no_impact category, 280 (33.1%) in stressed category, 40 (4.7%) in impacted category and 3 (0.4%) in degraded category in 2001. The number of basins within stressed category increased by 92 from 280 (33.1%) in 2001 to 372 (43.9%) in 2012. The number of drainage basins within impacted category increased by 17 from 40 (4.7%) in 2001 to 57 (6.7%) in 2012. Interestingly, it was found that in 2001, 43 (5.1%) drainage basins were already in the impacted and degraded categories, and this number increased by 21 to 64 (7.6%) in 2012. Overall, the number of drainage basins in the stressed, impacted and degraded categories is on an increasing trend over the period from 2001 to 2012. In contrast, the number of drainage basins within the no_impact category is on a decreasing trend (Figure 4.8). There were 524 (61.9%) drainage basins within the no_impact category in 2001, but the number was only 411 (48.5%) in 2012, a significant drop by 113. This change in severity of the basins was probably due to significant land development in these basins. These 113 normal basins became the stressed basins in 2012, contributing to a total of 372 stressed basins in 2012. As mentioned earlier, ISA at both the region and the country levels is on an increasing trend and is expected to continue to increase following the ISA trends (Figures 4.5 and 4.6). These results suggest that there is an urgent need to take appropriate measures to control the ISA growth in order to protect the basins' quality in the region, especially for the stressed basins before they fall into a more serious category. Furthermore, the currently normal basins should be carefully managed and considered (with other factors) in the urban land development plans because these basins can easily become stressed from the development pressure.

In examining each year's data, there were some drainage basins with the shift from more severe to less severe categories and vice-versa. For example, in 2002 there were 48 impacted basins, but in 2003 there were only 41 impacted basins. It was found that 11 of the impacted basins in

2002 turned to stressed basins in 2003, while the other 37 remained as impacted basins in 2003. In addition, the 4 of degraded basins in 2002 turned to impacted basins in 2003. The sum of two numbers (37 + 4) is 41, which is exactly the number of impacted basins in 2003. The 11 impacted basins in 2002 that turned to stressed basins in 2003 all had an ISA percentages of around 7% to 10%, whereas the 4 damaged basins in 2002 that changed the status to impacted category in 2003 all had an ISA percentage of around 27%. The ISA percentages are close to the thresholds that divide two adjacent categories (i.e. 10% and 25% respectively).

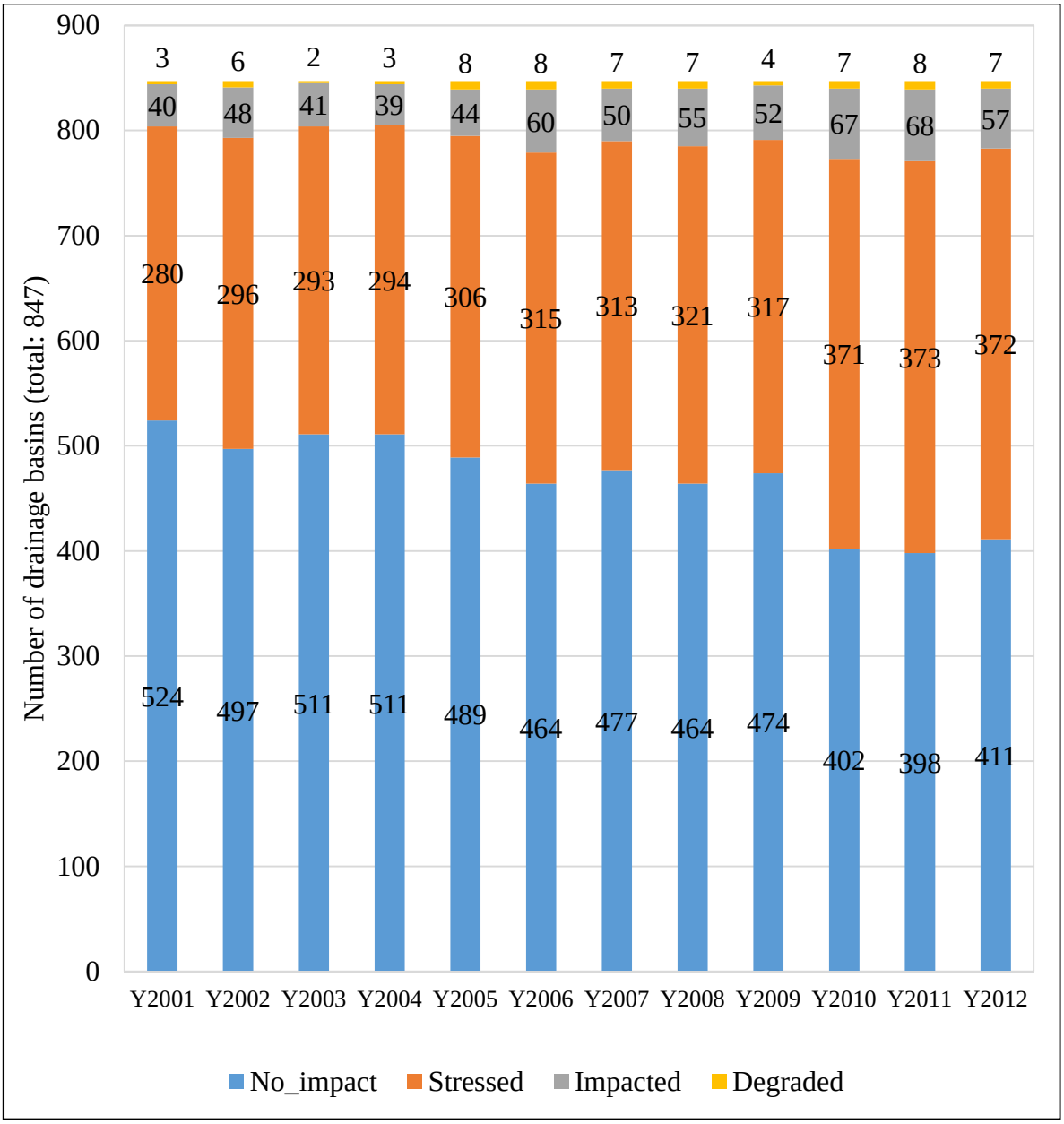

Figure 4. 7 Number of drainage basin classified by impact level from 2001 to 2012.

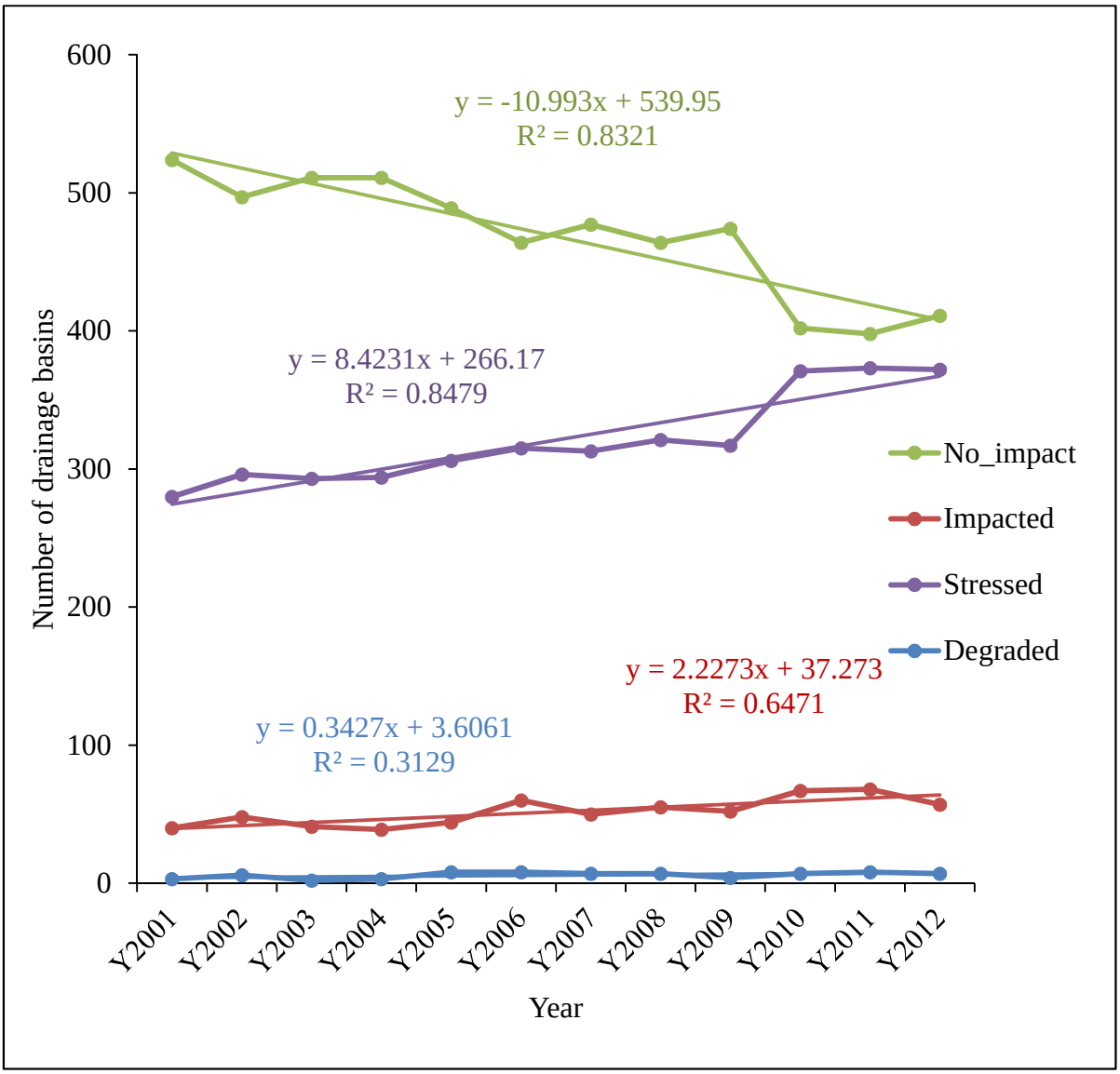

Figure 4. 8 Trends in the number of drainage basins for each category

Figure 4.9 illustrates the distribution maps of drainage basins classified by impact category in the lower Mekong region from 2001 to 2012. The three degraded drainage basins in 2001 were located in Bangkok metropolitan area, Thailand. In 2012, another one basin in Bangkok and three basins in Ho Chi Minh, Vietnam fell into the degraded category. This shift in the severity of impact to the degraded category occurred in suburban areas because of land development were expanded from the core areas. The ISA increased not only in the suburban areas of capitals of Bangkok and Ho Chi Minh, but also in other smaller cities of Thailand and Vietnam. In these smaller cities, some of the stressed basins shifted to the impacted basins. Overall, the effects of ISA on drainage

basins were found the most in Thailand with the basins within impacted category and stressed category accounting for a majority of the total basins (yellow and green colors in Figure 4.9). The drainage basins in Vietnam were also largely affected by ISA. As can be seen in Figure 4.9, the effects of ISA on the drainage basins in Cambodia and Laos were not significant. There were only a few basins in the stressed category, and no basins within impacted and degraded categories were found in both countries.

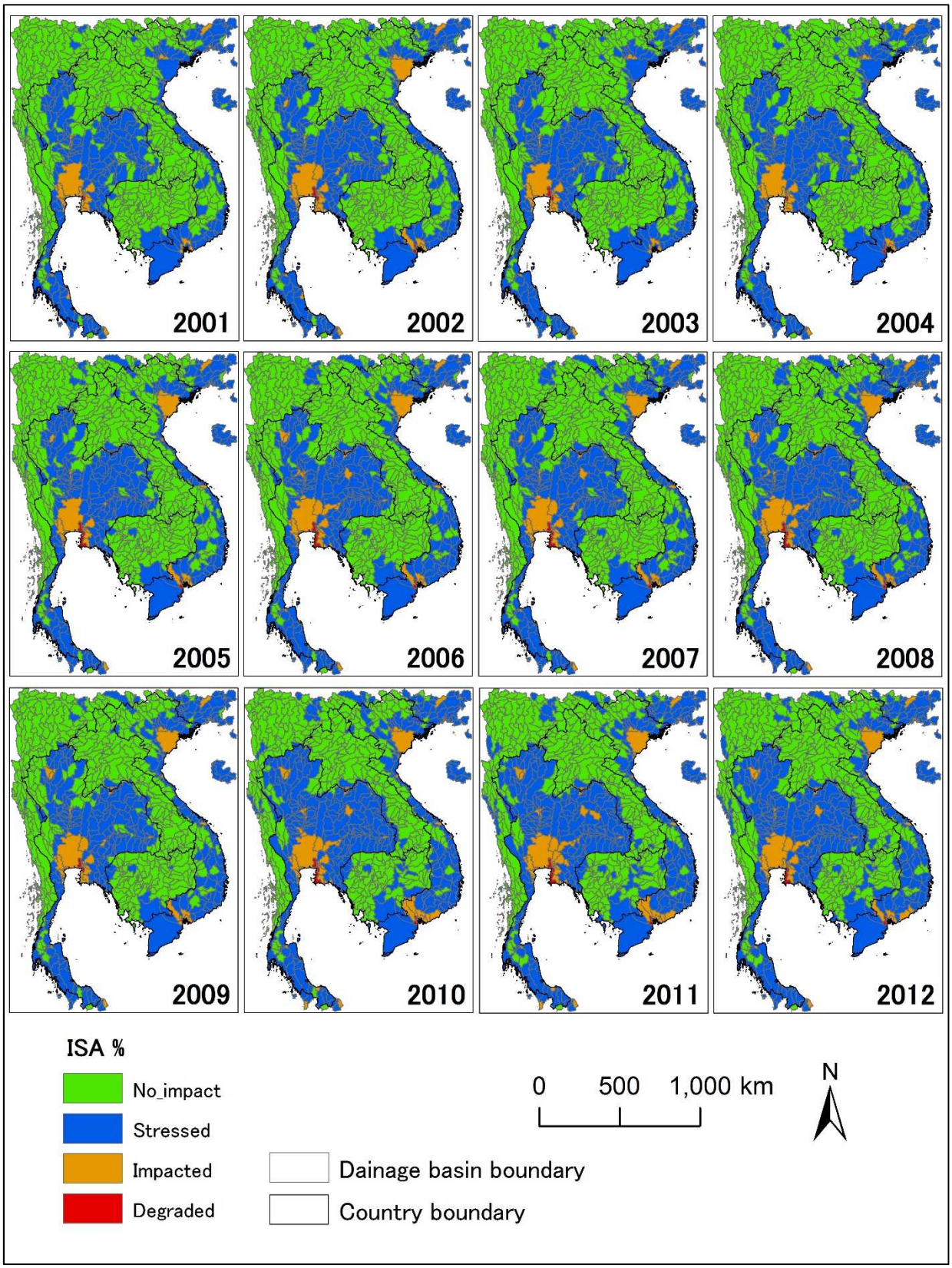

Figure 4. 9 Impact level of the drainage basins from 2001 to 2012

4.5 Discussion

4.5.1 Applicability of the ISA estimation method

In this study, annual ISA maps for the lower Mekong region from 2001 to 2012 were produced by using the method proposed in Chapter 3. The key element of the method lies in building a relationship between ISA and improved nighttime light (i.e. EANTLI). The two relationships (natural logarithmic function and second order polynomial function) between ISA and EANTLI were found for all the years from 2001 to 2012. This means the method was well applicable to estimate ISA for different years. However, the two relationships slightly differed, and the EANTLI values at the breakpoint between the two relationships slightly varied. This implies that it is required to build the relationships year by year for estimating ISA. It can be considered that the quality of input data of both MODIS and DMSP-OLS nighttime light may vary from year to year. Although efforts were made to improve data quality and comparability of the yearly data, they may not be perfect to remove all the effects in the data.

Application of the method to estimate ISA for other regions or for the entire world still needs to be explored. Two relationships between ISA and improved NTL were found in the study area (lower Mekong region), but the relationships may be different in other regions due to different light use efficiency and economic development that cause NTL value to be different. Moreover, the performance of TMA model for estimating the non-vegetation fraction to be used as the input for the above relationships is strongly dependent on the endmembers which tends to be different from one region to another. Fluctuations in the total ISAs estimated from the developed method for the twelve years from 2001 to 2012 were observed. It can be considered that ISA change estimated using two single years can be prone to large errors. Therefore, this study took the advantages of the richness of data to estimate ISA change. The linear regression models derived from the estimated ISA data of the 12 years ($R^2 > 0.67$ for the whole lower Mekong region and

the four countries) was used to estimate the change rate of ISA at regional and country levels with expectation to improve accuracy of ISA change.

The accuracy assessment results in Chapter 3 showed that the ISA estimated from the proposed method agrees well (R^2 = 0.87) with the ISA estimated from Google Earth images. In this chapter, the accuracy assessment was not carried other years. The impacts of ISA on the drainage basins in the whole study area were identified based on the percentage of ISA in each basin. However, considering the remaining errors and the size of basins, the ISA mapping results may not be effective for small basins. This is the reason that a few basins shifted from a more severe category to less severe category. The annual basin status maps can be useful to cross check the results and identify such basins. Then, if necessary, re-estimation of ISA for those specific basins can be done using Landsat or other high resolution images.

4.5.2 Sources of errors and uncertainties for ISA estimation

There are several sources of errors in the ISA estimations in this study. First is the OLS sensor differences. The sensors degrade over time, which affect the image quality. The inter-calibration and further correction using assumption that NTL in the previous year should not disappear in the following years were designed to reduce as many of these effects as possible. However, Elvidge et al. (2009) pointed out that the effects due to differences in the spectral bandpasses of the different OLS sensors may not be fully solved by performing inter-calibration. Further correction was performed to the inter-calibrated data to improve the comparability of the NTL data. However, images captured by the OLS-sensors may have over- and under-detection of lights across the years. For instance, NTL was detected in previous year, but was not detected in later years. It is uncertain that which year is correct. If the previous year's image is correct, then the assumption can address the issue. However, if the previous year is not correct, then our assumption cannot address the issue and the ISA result of the later years is overestimated.

Another consideration for the ISA estimation error is the nighttime light use in relation to economic activity, lifestyle and energy supply. Different countries may have different life use efficiency. According to Bennett and Smith (2017), the overpass time of the OLS sensor occurs during 20:30-21:30. Thus, lights illuminated during this period are determined by the way people work, live and enjoy. Furthermore, the energy source and supply can contribute to the estimation errors. For instance, in some places where there were no access to electricity in the past but after some years they could access to electricity, no light were captured by the OLS sensors, resulting in underestimation of ISA. In addition, the duration that the light is turned on at night may be short in some areas especially rural areas and may be different from the time when the satellite cross over. Although, the nighttime light data used in this study was the annual stable lights composites which can maintain the light even if there is cloud obstruction or light on the ground is turned off on some days in a year, the nighttime light images may suffer this effect of different nighttime light use and cause errors in ISA estimation from year to year.

Moreover, previous studies using DMSP-OLS NTL data have found that the data tend to exaggerate the size of the urban extent due to the reason that nighttime light features derived by OLS sensors are substantially larger than the lighting sources on the ground and thus determined threshold of NTL to extract urban extents (Zhou et al., 2015). Using the thresholding technique, pixels with NTL value less than the threshold were not classified as urban area. However, the present study did not apply threshold to map ISA. It should be noted that the definition of urban area or extent is different from ISA. In this present study, ISA is defined as human-made surfaces such as housings, buildings, roads and parking lots. These types of impervious surfaces not only contain in urban areas, but also in rural areas. Therefore, if a threshold is applied to the NTL data, the rural areas or undeveloped areas where light intensity is usually low will disappear in the ISA maps. Moreover, low-lighted rural areas or sub-urban areas can contain large amount of ISA because a lot of land development activities focus on roads and low-rise buildings, rather than high-rise buildings.

MODIS NDVI data were used in the TMA to estimate non-vegetation fraction for each year. Inter-annual variability of NDVI time-series could be another source of errors in the ISA change. The inter-annual variation can be caused by meteorological distortions like clouds and environmental process like effects of variations in weather conditions on plant growth from year to year (Forkel et al., 2013). Although the downloaded MODIS NDVI product was a 16-day composite of high quality pixels and efforts was made on smoothing the NDVI time-series in each year to minimize the remaining effects of clouds and noise, they only improved the intra-annual variability. However, the inter-annual variation may remain high (Clark et al., 2012). This may be considered the limitation of this study. A future study should look into this issue to see how the inter-variability of NDVI affects the ISA changes and how to reduce this variability.

Another source that may cause the fluctuation of annual ISA data during 2001-2012 is the number of pixels with No Data value in the MODIS NDVI time-series. In this study, 16-day composites of NDVI data for one year (i.e. 23 images per year) was used in the TMA to estimate non-vegetation fraction. These 23 images originally have slightly different number of pixels with No Data value. In this study, the pixels that have No Data in one of the 23 images of the year were discarded and not used for compuation. This process was implemented for the twelve years, resulting in different numbers of pixels with No Data value for all twelve years. For the twelve years, the percentages of pixels with No Data value were 40.72% (lowest percentage among the twelve years) in 2002 and 40.96% (highest percentage) in 2005. The difference between the highest and lowest percentages was 0.24% of the total pixels. Although the difference of these pixels is small, it may in part contribute to the fluctuation in the ISA change over time. For example, in urban areas located near the coastlines, it is observed that there are pixels that have No Data value in some images, but do not have No Data value in other images.

4.5.3 Potential forces for shift in severity of ISA impacts on drainage basins

The ISA results were overlaid with the drainage basin boundary for identifying the impact status of the drainage basins. This research showed the distribution of drainage basins classified by the impact level in the lower Mekong region. This information can be subsequently used to make management policies or measures related to watersheds and water quality which is important to human health. The drainage basins in degraded and impacted categories are located in cities or suburban areas. Many studies have suggested regulating the ISA within 10% in drainage basin to reduce the degradation of water quality and protect the overall drainage basin (e.g. Theobald et al., 2009; Kim et al., 2016). The characteristics of land development is strongly related to the increase in the amount of ISA. The shift in category of drainage basins may be driven by the conversion of agricultural and forest lands in the suburban areas into impervious surfaces. Population growth and fast development were two main forces of increase in ISA in the study area. The inflow of foreign investments plays an important role as the countries in the lower Mekong region has a lot of young labor forces and relatively cheap labor cost. Consequently, a lot of factories, buildings and other infrastructure have been built. Furthermore, the construction of roads and highways to meet the transportation demands of rising population and economic activities has led to the ISA increase and thus causing the shift in severity of ISA impact on drainage basins. Controlling the amount of ISA to remain low is important to protect the drainage basin that are still in the no_impact and stressed categories.

4.6 Conclusions

In this study, annual ISA% maps from 2001 to 2012 for the lower Mekong region were produced to assess changes of ISA and its impacts on drainage basins. The analysis results revealed a significant increase in ISA in the lower Mekong region over the twelve years' period from 2001 to 2012. The method was well applicable and it was required to build relationships between ISA

and EANTLI year by year. The method provides a relatively easy and cost-effective means to monitor ISA over a large area. Using the ISA maps from 2001 to 2012, the status of drainage basins and water quality were assessed in the lower Mekong region. The drainage basins were classified into four categories based on the percentage of ISA in the drainage basin: no_impact, stressed, impacted and degraded. The impact of ISA in the region was noticeable with 5% of the basins already within the impacted and degraded categories in 2001. Significant impacts were found in Thailand and Vietnam. Over the years, the shift from impacted to degraded category occurred in the drainage basins adjacent to Bangkok and Ho Chi Minh metropolitans, whereas the shift from stressed to impacted category occurred not only in near the metropolitan areas, but also in the other smaller cities, mainly in Thailand and Vietnam. The study is useful for rapidly mapping and updating ISA as well as for identifying the severity of ISA impacts on drainage basins. This information can be used to develop policies and take appropriate measures to manage ISA growth and to protect the quality of drainage basins.

Chapter 5

General conclusions

5.1 Summary

A simple, cost-effective and easy-to-implement method was developed for estimating ISA% on a large scale. The developed method involves four major steps and requires coarse spatial resolution data from MODIS and DMSP-OLS NTL. The four major steps are: (1) estimate the non-vegetation fraction from MODIS NDVI time-series products using the TMA method; (2) obtain improved NTL data by calculating EANTLI from the monthly MODIS EVI product and DMSP-OLS NTL data; (3) generate a preliminary ISA% map by building a relationship between ISA% and EANTLI based on the statistical analysis of the maps from the first and second steps; (4) obtain a final ISA% map by comparing the preliminary ISA% map to the non-vegetation fraction map and selecting the smaller values. The validation result showed that the developed method has promising accuracy for estimating the ISA% for the lower Mekong region, with an RMSE value of 0.111, an SE value of 0.061, and a determination coefficient of 0.87. Another important finding is that there were two relationships between ISA% and the improved NTL (i.e., EANTLI): the natural logarithmic function is suitable for ISA% values between 0 and 50%, and the quadratic polynomial function should be used for ISA% values larger than 50%. The developed method shows high potential for use in generating a global ISA% map with frequent updates because of its easy implementation and readily available input data.

Twelve annual ISA% maps from 2001 to 2012 for the lower Mekong region were produced using the developed method. The relationships between ISA% and EANTLI for all the years were similar, with slight difference. This indicates that the relationships should be built year by year. Differences in the relationships can be considered due to the varied quality of input data namely

MODIS and DMSP-OLS NTL. Although improvements of the data were made in this study, the effects may not be completely reduced. The changes in ISA over the lower Mekong region and for each country within the region were presented. A key aspect of this analysis was to make full use of the annual ISA data to generate the linear trend model, anticipating to improve the accuracy. The analysis results revealed a substantial increase in ISA in the region over the period from 2001 to 2012. In addition, the extent of increase was largely contributed by Thailand and Vietnam. More attention should be paid to the environmental effects of the increased ISA in the lower Mekong region. In addition, the information is a valuable source for regional planning and management, and evaluating environmental impacts on drainage basins in the region. The method provides a relatively easy, quick and cost-effective means to annually monitor ISA over a large area.

Because ISA is an important indicator of drainage basin quality, the ISA maps were used to generate the maps showing status of the drainage basins in the region. First, the ISA was extracted for each basin and the percentage of ISA relative to the basin area was calculated for each year from 2001 to 2012. Then, the basins were classified into four categories according to the basins' percentages of ISA: no_impact (percentage of ISA less than 1%), stressed (percentage of ISA between 1% and 10%), impacted (percentage of ISA between >10% and 25%) and degraded (percentage of ISA larger than 25%). The analysis showed that of a total of 847 drainage basins in the lower Mekong region, there were 524 (61.9%) in no_impact category, 280 (33.1%) in stressed category, 40 (4.7%) in impacted category and 3 (0.4%) in degraded category in 2001. After eleven years, the number of drainage basins that used to function normally decreased by up to 113 from 524 to 411. Contrary to that, the number of basins in stressed, impacted and degraded categories increased to 372, 57 and 7 respectively in 2012. The shift to a more severe category was observed in not only suburban areas of large metropolitan areas, but also in small cities. These results suggest that there is an urgent need to take appropriate measures to control the ISA growth in order

to protect the basins' quality in the region, especially for the stressed basins before they fall into a more serious category.

5.2 Significance of this research

The first contribution of this research lies in the successful integration of improved DMSP-OLS NTL data with TMA-based ISA estimation method to overcome the issue of confusion between temporal signatures of bare land and ISA. In TMA, ISA tends to be misestimated as bare land, so accurate ISA fraction cannot be directly obtained. As it is well known that NTL intensity is a strong indicator of urbanization or human settlements, NTL data are useful in estimating ISA. However, the original DMSP-OLS NTL image is often suffered by saturation in bright urban areas and blooming in the sub-urban areas. After mitigating these two problems, the improved DMSP-OLS NTL data enabled a more efficient reduction of bare land effects.

Another contribution is the utilization of non-vegetation fraction derived from TMA to establish relationships between ISA and improved nighttime light. The non-vegetation fraction map from TMA also contains accurate ISA pixels for the areas that are not affected by bare land. In this research, a statistical analysis was performed on this non-vegetation fraction and the improved nighttime light to find these ISA pixels and build the relationships. Then, ISA fraction map with minimized effects of bare land was generated from the relationships. As a result, the accuracy has been improved. In building the relationships for estimating ISA, past studies generally suffered difficulties in processing big data from Landsat or other satellites with higher spatial resolution to generate reference ISA data, which is laborious and computationally intensive as well as difficulties in selecting an area or a number of samples that can appropriately represent the other areas. This research does not requires Landsat data and can simplify the representability issue by just using the non-vegetation fraction map of the whole study area. Therefore, this research is useful as it provides a procedure that is relatively easy to implement, cost-effective and can quickly and frequently estimate and monitor ISA in our rapidly urbanizing world.

The third contribution of this research is that twelve annual maps of ISA for lower Mekong region have been produced and analyzed at various spatial scales (regional and national), and the impacts on drainage basins presented. In doing so, efforts were made on enhancing the temporal consistency of DMSP-OLS NTL time-series prior to applying the developed method to create the ISA maps. A substantial increase in ISA was revealed, reflecting the rapid urbanization in the lower Mekong region. The data of ISA and status of drainage basins at high temporal frequency (annual) are critical for decision makers, urban planners, drainage basin managers and scientists in related fields who are interested in studying the lower Mekong region.

5.3 Future research directions

The applicability of the method developed in this research should be tested in other regions or the world. Due to the demand for up-to-date information about ISA, the use of new nighttime light data from Suomi NPP-VIIRS satellite instead of DMSP-OLS NTL in the developed method should be explored. The use of NOAA AVHRR's NDVI data instead of MODIS EVI in the EANTLI equation should be explored because if successful it is possible to apply the method to generate ISA maps in the past. Moreover, future research should be conducted in a comprehensive way on how the regional and national development policies affect the ISA change that lead to the shifts in the impact category of the drainage basins.

Acknowledgements

First of all, I would like to express my sincere thanks to my supervisor, Prof. Bunkei Matsushita for his valuable advice, guidance and encouragement throughout my study. I am very grateful for his great scientific discussions which greatly helped me to make the continuous progress and to complete this dissertation.

I would also like to acknowledge Prof. Kenlo Nishida Nasahara, Prof. Yuji Murayama, Prof. Hiroaki Kato, Prof. Yuichi Onda, and Emeritus Prof. Takehiko Fukushima for their valuable comments to improve my research and dissertation.

Many thanks go to all the members of my lab for their friendliness, kind assistance and a pleasant learning environment during my study.

I must express my gratitude to my parents, brothers and sisters who have been supporting and encouraging me until now. All their support and understanding mean a lot to me.

Finally, I would like to greatly thank the Ministry of Education, Culture, Sports, Science and Technology, Japan for providing the scholarship which allowed me to undertake my studies and research in this beautiful and amazing country.

References

1. Alberti, M., Booth, D., Hill, K., Coburn B., Avolio, C., Coe, S., Spirandelli, D. The impact of urban patterns on aquatic ecosystems: An empirical analysis in Puget lowland sub-basins. *Landscape and Urban Planning*, 80 (4), 2007, 345-361

2. Arnold, C.L., & Gibbons, C.J. (1996). Impervious surface coverage: the emergence of a key environmental indicator. *Journal of American Planning Association*, 62 (2), 243-258.

3. Bauer, M.E., Loffelholz, B.C., Wilson, B., (2008). Estimating and mapping impervious surface area by regression analysis of Landsat imagery. In: Weng, Q., (Ed.), Remote Sensing of Impervious Surfaces, CRC Press, Boca Raton, FL, USA, pp. 3– 19.

4. Bennie, J., Davies, T.W., Duffy, J.P., Inger, R., & Gaston, K.J. (2014). Contrasting trends in light pollution across Europe based on satellite observed night time lights. *Scientific Reports*, 4, 3789.

5. Bennett, M,M, & Smith, L.C. (2017). Advances in using multitemporal night-time lights satellite imagery to detect, estimate, and monitor socioeconomic dynamics. *Remote Sensing of Environment*, 192, 176-197.

6. Bierwagen, B.G., Theobald, D.M., Pyke, C.R., Choate, A., Groth, P., Thomas, J.V., & Morefield, P. (2010). National housing and impervious surface scenarios for integrated climate impact assessments. *Proceedings of the National Academy of Sciences*, 107 (49) 20887-20892

7. Buyantuyev, A. & Wu, J. (2010). Urban heat islands and landscape heterogeneity: linking spatiotemporal variations in surface temperatures to land-cover and socioeconomic patterns. *Landscape Ecology*, 25 (1), 17-33.

8. Cauwels, P.; Pestalozzi, N.; Sornette, D. (2014). Dynamics and spatial distribution of global nighttime lights. *EPJ Data Science*, 3, 1–26.

9. Chen, J., Jönsson, P., Tamura, M., Gu, Z., Matsushita, B., & Eklundh, L. (2004). A simple method for reconstructing a high-quality NDVI time-series data set based on the Savitzky–Golay filter. *Remote Sensing of Environment*, 91, 332-344.

10. Clark M.L., Aide T.M., & Riner G. (2012). Land change for all municipalities in Latin America and the Caribbean assessed from 250 m MODIS imagery (2001–2010). *Remote Sensing of Environment*, 126, 84–103

11. Du, S., Shi, P., Van Rompaey, A., & Wen, J. (2015). Quantifying the impact of impervious surface location on flood peak discharge in urban areas. *Natural Hazards*, 76, 1457–1471.

12. Elvidge, C.D.; Baugh, K.E.; Kihn, E.A.; Kroehl, H.W. & Davis, E.R. (1997). Mapping city lights with nighttime data from the DMSP Operational Linescan System. *Photogrammetric Engineering and Remote Sensing*, 63, 727-734.

13. Elvidge, C.D., Tuttle, T.B., Sutton, C.P., Baugh, E.K., Howard, T.A., Milesi, C., Bhaduri, B., & Nemani, R. (2007). Global Distribution and Density of Constructed Impervious Surfaces. *Sensors*, 7, 1962-1979.

14. Elvidge, C.D., Ziskin, D., Baugh, K.E., Tuttle, B.T., Ghosh, T., Pack D.W., Erwin, E.H., & Zhizhin, M. (2009). A fifteen year record of global natural gas flaring derived from satellite data. *Energies*, 2, 595-622.

15. Elvidge, C.D., Hsu, F.-C., Baugh, K. & Ghosh, T. (2014). National trends in satellite-observed lighting: 1992-2012. In Weng, Q. (Ed.) *Global Urban Monitoring and Assessment Through Earth Observation*, CRC Press, Boca Raton.

16. Forkel, M., Carvalhais, N., Verbesselt, J., Mahecha, M.D., Neigh, C.S., & Reichstein, M. (2013). Trend Change Detection in NDVI Time Series: Effects of Inter-Annual Variability and Methodology. *Remote Sensing*, 5, 2113-2144.

17. Gallo, K., & Xian, G., 2016. Changes in satellite-derived impervious surface area at US historical climatology network stations. *ISPRS Journal of Photogrammetry and Remote Sensing*, 120, 77-83.

18. Grimm, N.B., Faeth, S.H., Golubiewski, N.E., Redman, C.L., Wu, J., Bai, X., & Briggs, J.M. (2008). Global change and the ecology of cities. *Science,* 319 (5864), 756–760.

19. Huang, X., Schneider, A., & Friedl, M.A. (2016). Mapping sub-pixel urban expansion in China using MODIS and DMSP/OLS nighttime lights. *Remote Sensing of Environment*, 175, 92-108.

20. Jacobson, C.R. (2011). Identification and quantification of the hydrological impacts of imperviousness in urban catchments: A review. *Journal of Environmental Management*, 92 (6), 1438-1448.

21. Kim, H., Jeong, H., Jeon, J., & Bae, S., (2016). The impact of impervious surface on water quality and its threshold in Korea. *Water,* 8, 111.

22. Kuang, W. H., Liu, J. Y., Zhang, Z. X., Lu, D. S. & Xiang, B. (2013). *Spatiotemporal dynamics of impervious surface areas across China during the early 21st century*. Chinese Science Bulletin, 58, 1691–1701.

23. Knight, J. & Voth, M. (2011). Mapping impervious cover using multi-temporal MODIS NDVI data. *IEEE Journal of Selected Topics in Applied Earth Observations and Remote Sensing*, 4, 303-309.

24. Klein, R. (1979). "Urbanization and Stream Quality Impairment." American Water Resources Association. *Water Resources Bulletin*, 15(4).

25. Le Moigne, J., Netanyahu, N. S., & Eastman, R. D. (Eds.). (2011). *Image Registration for Remote Sensing*. Cambridge: Cambridge University Press.

26. Lee, S., & Lathrop, R. G. (2006). Subpixel analysis of Landsat ETM+ using Self-Organizing Map (SOM) neural networks for urban land cover characterization. *IEEE Transactions on Geoscience and Remote Sensing*, 44(6), 1642-1654.

27. Li, J., Song, C., Cao, L., Zhu, F., Meng, X., & Wu, J. (2011). Impacts of landscape structure on surface urban heat islands: A case study of Shanghai, China. *Remote Sensing of Environment*, 115 (12), 3249-3263.

28. Li, W. & Wu, C. (2015). Incorporating land use land cover probability information into endmember class selections for temporal mixture analysis. *ISPRS Journal of Photogrammetry and Remote Sensing*. 101, 163-173.

29. Li, X. & Zhou, Y., (2017). A Stepwise Calibration of Global DMSP/OLS Stable Nighttime Light Data (1992–2013). *Remote Sensing*, 9(6), 637.

30. Liu, Z., Wang, Y., Li, Z., Peng, J. (2013). Impervious surface impact on water quality in the process of rapid urbanization in Shenzhen, China. *Environmental Earth Sciences*, 68, 2365–2373.

31. Liu, X., Hu, G., Ai, B., Li, X., & Shi, Q. (2015). A Normalized Urban Areas Composite Index (NUACI) Based on Combination of DMSP-OLS and MODIS for Mapping Impervious Surface Area. *Remote Sensing*, 7, 17168-17189.

32. Lu, D., Tian, H., Zhou, G., & Ge, H. (2008). Regional mapping of human settlements in southeastern China with multisensor remotely sensed data. *Remote Sensing of Environment*, 112, 3668-3679.

33. Lu, D., & Weng, Q. (2006). Use of impervious surface in urban land-use classification. *Remote Sensing of Environment*, 102, 146-160.

34. MRC (2011). Planning atlas of the Lower Mekong River Basin. Mekong River Commission, Phnom Penh, Cambodia.

35. MRC (2010). State of the basin report 2010. Mekong River Commission, Vientiane, Lao PDR.

36. Matsushita, B., Yang, F., & Fukushima, T. (2014). Impervious surface area as an indicator for evaluating drainage basins. In Nakano, S.-i, Yahara, T., & Nakashizuka, T. (Ed.), *Integrative Observations and Assessments, Ecological Research Monographs*, Springer Japan.

37. Murayama, Y., Estoque, R.C., Hou, H., Gong, H., Simwanda, M., Subasinghe, H., & Zhang, X. (2016). Visualization of land-use/land-cover changes in major Asian and African cities. *Annual Report on the Multi Use Social and Economic Data Bank*, p. 95. Website: http://giswin.geo.tsukuba.ac.jp/mega-cities/.

38. Novak, J.D., & Greenfield, J.E. (2012). Tree and impervious cover in the United States. *Landscape and Urban Planning*, 107 (1), 21-30.

39. Pandey B., Zhang Q., Seto K.C. (2017). Comparative evaluation of relative calibration methods for DMSP/OLS nighttime lights. *Remote Sensing of Environment*, 195, 67-78.

40. Pok, S., Matsushita, B., & Fukushima, T. (2017). An easily implemented method to estimate impervious surface area on a large scale from MODIS time-series and improved DMSP-OLS nighttime light data. *ISPRS Journal of Photogrammetry and Remote Sensing*, 133, 104-115.

41. Powell, R.L., Roberts, D.A., Dennison, P.E., & Hess, L.L. (2007). Sub-pixel mapping of urban land cover using multiple endmember spectral mixture analysis: Manaus, Brazil. *Remote Sensing of Environment*, 106, 253-267.

42. Ridd, M.K. (1995). Exploring a V-I-S (vegetation-impervious surface-soil) model for urban ecosystem analysis through remote sensing: comparative anatomy for cities. *International Journal of Remote Sensing* 16 (12), 2165-2185.

43. Shao, Y. & Lunetta, R.S. (2011). Sub-pixel mapping of tree canopy, impervious surfaces, and cropland in the Laurentian Great Lakes Basin using MODIS time-series data. *IEEE Journal of Selected Topics in Applied Earth Observations and Remote Sensing*, 4 (2), 336-347.

44. Schueler, T. R. (1994). The importance of imperviousness. *Watershed Protection Techniques*, 1 (3), 100-111.

45. Schueler, T.R., Fraley-McNeal, L., & Cappiella, K. (2009). Is impervious cover still important? Review of recent research. *Journal of Hydrologic Engineering*, 14, 309–315.

46. Shuster,W.D., Bonta, J., Thurstron, H.,Warnemuende, E., & Smith, D.R. (2005). Impacts of impervious surface on watershed hydrology: A review. *Urban Water Journal*, 2, 263–275.

47. Slonecker, T.E., Jennings, B.D., & Garofalo, D. (2001). Remote sensing of impervious surfaces: A review. *Remote Sensing Reviews*, 20 (3), 227-255.

48. Small, C., Pozzi, F., & Elvidge, C.D. (2005). Spatial analysis of global urban extent from DMSP-OLS night lights. *Remote Sensing of Environment*, 96, 277–291.

49. Small, C., & Elvidge, C. D. (2013). Night on Earth: mapping decadal changes of anthropogenic night light in Asia. *International Journal of Applied Earth Observation and Geoinformation*, 22, 40–52.

50. Somers, B., Asner, G.P., Tits, L., & Coppin, P. (2011). Endmember variability in spectral mixture analysis: A review. *Remote Sensing of Environment*, 115, 1603-1616.

51. Theobald, D.M., Goetz, S.J., Norman, J, B, & Jantz, P. (2009). Watersheds at risk to increased impervious surface cover in the Conterminous United State. *Journal of Hydrologic Engineering*, 14 (4), 362-368.

52. United Nations, Department of Economic and Social Affairs, Population Division (2014). World Urbanization Prospects: The 2014 Revision, Highlights (ST/ESA/SER.A/352).

53. Weng, Q. (2012). Remote sensing of impervious surfaces in the urban areas: Requirements, methods, and trends. *Remote Sensing of Environment*, 117, 34-49.

54. Weng, Q., & Hu, X. (2008). Medium spatial resolution satellite imagery for estimating and mapping urban impervious surfaces using LSMA and ANN. *IEEE Transaction on Geoscience and Remote Sensing*, 46(8), 2397-2406.

55. Wu, C. (2004). Normalized spectral mixture analysis for monitoring urban composition using ETM+ imagery. *Remote Sensing of Environment*, 93, 480-492.

56. Wu, C., & Murray, A.T. (2003). Estimating impervious surface distribution by spectral mixture analysis. *Remote Sensing of Environment*, 84, 493-505.

57. Xian, G., Crane, M., & Su, J. (2007). An analysis of urban development and its environmental impact on the Tempa Bay watershed. *Journal of Environmental Management*, 85, 965-976.

58. Xian, G., & Homer, C. (2010). Updating the 2001 national land cover database impervious surface products to 2006 using Landsat imagery change detection methods. *Remote Sensing of Environment*, 114(8), 1676-1686.

59. Xie, Y., & Weng, Q., (2017). Spatiotemporally enhancing time-series DMSP/OLS nighttime light imagery for assessing large-scale urban dynamics. *ISPRS Journal of Photogrammetry Remote Sensing*, 128, 1–15.

60. Yang, F., Matsushita, B., & Fukushima, T. (2010). A pre-screened and normalized multiple endmember spectral mixture analysis for mapping impervious surface area in Lake Kasumigaura Basin, Japan. *ISPRS Journal of Photogrammetry and Remote Sensing*, 65, 479-490.

61. Yang, F., Matsushita, B., Fukushima, T., & Yang, W. (2012). Temporal mixture analysis for estimating impervious surface area from multi-temporal MODIS NDVI data in Japan. *ISPRS Journal of Photogrammetry and Remote Sensing*, 72, 90-98.

62. Yang, F., Matsushita, B., Yang, W., & Fukushima, T. (2014). Mapping the human footprint from satellite measurements in Japan. *ISPRS Journal of Photogrammetry and Remote Sensing*, 88, 80-90.

63. Zhang, Q., & Seto, K.C. (2011). Mapping urbanization dynamics at regional and global scales using multi-temporal DMSP/OLS nighttime light data. *Remote Sensing of Environment*, 115 (9), 2320-2329

64. Zhang, Q., Schaaf, C., & Seto, K.C. (2013). The Vegetation Adjusted NTL Urban Index: A new approach to reduce saturation and increase variation in nighttime luminosity. *Remote Sensing of Environment*, 129, 32-41.

65. Zhang, Q., Pandey, B., & Seto, K. C. (2016). A robust method to generate a consistent time series from DMSP/OLS nighttime light data. *IEEE Transactions on Geoscience and Remote Sensing*, 54(10), 5821 – 5831.

66. Zhou, Y., Smith, S.J., Zhao, K., Imhoff, M., Thomson, A., Bond-Lamberty, B., Asrar, G.R., Zhang, X., He, C., Elvidge, C.D. (2015). A global map of urban extent from nightlights. *Environmental Research Letters*, 10, 054011.

67. Zhuo, L., Zheng, J., Zhang, X., Li, J., & Liu, L. (2015). An improved method of night-time light saturation reduction based on EVI. *International Journal of Remote Sensing*, 36, 4114-4130.

68. Zhu, H., Li, Y., Liu, Z., & Fu, B. (2015). Estimating the population distribution in a county area in China based on impervious surfaces. *Photogrammetric Engineering & Remote Sensing*, 81 (2), 155-163.